

1  
2  
3 **Understanding prefrontal cortex functions**  
4 **by decoding its molecular, cellular and circuit organization**

5  
6 Aritra Bhattacharjee<sup>1,2,3#</sup>, Chao Zhang<sup>1,2,3#</sup>, Brianna Watson<sup>2,4</sup>, Mohamed Nadhir Djekidel<sup>1,2,3,5</sup>,  
7 Jeffrey R. Moffitt<sup>2,4\*</sup> and Yi Zhang<sup>1,2,3,6,7\*</sup>  
8

9 <sup>1</sup>Howard Hughes Medical Institute, Boston Children's Hospital, Boston, Massachusetts 02115, USA;  
10 <sup>2</sup>Program in Cellular and Molecular Medicine, Boston Children's Hospital, Boston, Massachusetts  
11 02115, USA; <sup>3</sup>Division of Hematology/Oncology, Department of Pediatrics, Boston Children's Hospital,  
12 Boston, Massachusetts 02115, USA; <sup>4</sup>Department of Microbiology, Harvard Medical School, Boston,  
13 Massachusetts 02115, USA; <sup>5</sup>Center for Applied Bioinformatics, St. Jude Children's Research Hospital,  
14 262 Danny Thomas Place, Memphis, TN, 38105, USA; <sup>6</sup>Department of Genetics, Harvard Medical  
15 School, Boston, Massachusetts 02115, USA; <sup>7</sup>Harvard Stem Cell Institute, WAB-149G, 200 Longwood  
16 Avenue, Boston, Massachusetts 02115, USA.  
17

18 #These authors contributed to this work equally

19 \*To whom correspondence should be addressed

20 E-mail: [yzhang@genetics.med.harvard.edu](mailto:yzhang@genetics.med.harvard.edu)

21 [Jeffrey.Moffitt@childrens.harvard.edu](mailto:Jeffrey.Moffitt@childrens.harvard.edu)  
22  
23  
24

25 Running title: Spatial transcriptomics analysis of mouse PFC  
26  
27

28 Keywords: Mouse prefrontal cortex, spatial transcriptomics, MERFISH, neuron cluster projection, pain  
29  
30

31 Manuscript information: 36 pages, 6 figures, 8 supplemental figures, 3 supplemental tables  
32

33 **Abstract**

34

35 The prefrontal cortex (PFC) is functionally one of the most complex regions of mammalian  
36 brain. Unlike other cortical areas that process single sensory modalities (like vision, touch, smell, etc.),  
37 the PFC integrates information across brain regions to regulate diverse functions ranging from cognition,  
38 emotion, executive action to even pain sensitivity. However, it is unclear how such diverse functions are  
39 organized at the cellular and circuit levels within the anatomical modules of the PFC. Here we employed  
40 spatially resolved single-cell transcriptome profiling to decode PFC's organizational heterogeneity. The  
41 results revealed that PFC has very distinct cell type composition relative to all neighboring cortical  
42 areas. Interestingly, PFC also adopts specialized transcriptional features, different from all neighbors,  
43 with differentially expressed genes regulating neuronal excitability. The projections to major  
44 subcortical targets of PFC emerge from combinations of neuron subclusters determined in a target-  
45 intrinsic fashion. These cellular and molecular features further segregated within subregions of PFC,  
46 alluding to the subregion-specific specialization of several PFC functions. Finally, using these unique  
47 cellular, molecular and projection properties, we identified distinct cell types and circuits in PFC that  
48 engage in pathogenesis of chronic pain. Collectively, we not only present a comprehensive  
49 organizational map of the PFC, critical for supporting its diverse functions, but also reveal the cluster  
50 and circuit identity of a pathway underlying chronic pain, a rapidly escalating healthcare challenge  
51 limited by molecular understanding of maladaptive PFC circuits.

52

53

54 **Major points**

- 55 • PFC adopts unique cellular composition, distinct from other cortical areas
- 56 • Selective transcriptomic features emerge in PFC to support its divergent functional portfolio
- 57 • Subcortical projections of PFC assume target-intrinsic specification for innervating clusters
- 58 • A molecularly defined L5 projection neuron cluster (to PAG) potentially mediates chronic pain  
59 pathogenesis

60

61

62 **Introduction**

63

64 The prefrontal cortex (PFC) is a major region of the mammalian brain that has evolved to  
65 perform highly complex behavioral functions. It plays important roles in cognition, emotion and  
66 executive function. Unlike somatosensory, visual, auditory, motor or other cortices, which are unimodal  
67 (process single modalities like touch, vision, hearing, movement etc.), the PFC engages in complex  
68 executive tasks that dynamically coordinate cognition, attention, learning, memory, judgement, etc. to  
69 direct the action of an organism<sup>1,2</sup>. As such, dysfunctions of the PFC are associated with many cognitive  
70 and neuropsychiatric disorders<sup>3,4</sup>.

71 In addition to regulating intellectual and emotional behaviors, PFC is even involved in  
72 modulating pain sensitivity as well as the negative affect of pain<sup>5,6</sup>. Increasing evidence indicates that  
73 disruption of this regulation is associated with the development of chronic pain, a rapidly increasing  
74 healthcare challenge that affects about 20% of the US population, exceeding cost burden of diabetes or  
75 heart disease<sup>7,8</sup>. Chronic pain has been associated with PFC hypoactivity, and transcranial stimulation of  
76 the PFC can induce pain relief<sup>9-15</sup>. Although projections from PFC to brainstem has been historically  
77 described in descending inhibition of pain<sup>5,16,17</sup>, the underlying molecular mechanism is poorly  
78 characterized. Besides, PFC interacts with many downstream targets including the amygdala, nucleus  
79 accumbens and thalamus - the major components of the central pain matrix, critical for the sensory or  
80 affective symptoms of chronic pain<sup>6,18</sup>. As such, PFC plays an important role in pain “chronification”<sup>5,17</sup>.

81 Thus, a central question is how does PFC organize and manage such diverse functions: from  
82 cognitive processes to autonomic pain modulation? To address this question, we and others have  
83 previously performed single-cell RNA-seq (scRNA-seq) to decode the cellular heterogeneity of the  
84 PFC<sup>2,19</sup>, which revealed a myriad of cell types comprising PFC. However, those studies lacked  
85 information about the spatial organization and interaction of the diverse cell types, which are major  
86 determinants of the functional diversity of the PFC. A relatively homogeneous histology, with a laminar  
87 organization, is the most striking feature of the mammalian cerebral cortex<sup>20-22</sup>. Yet, distinct regions of  
88 cortex perform highly specialized functions, including vision, locomotion, and somatosensation, etc.  
89 This regional specialization of functions, despite apparent homogeneity, must be due to distinct features  
90 at multiple levels including - molecular composition (transcriptome), circuit organization (connectome)  
91 and anatomical (spatial) organization of cell subtypes within each cortical area. Decoding such  
92 organizational logic is critical not only for mechanistic understanding of cortical function, but also for

93 developing drugs to selectively target neurological disorders of cortical origin, such that drugs directed  
94 for either cognitive (frontal cortex) or hearing (auditory cortex) defect, do not disrupt visual or motor  
95 function.

96         Approaching such questions has been historically limited by technological barriers, despite  
97 extensive scRNAseq profiling across brain, including cortex<sup>23-25</sup>. However, with recent advances in  
98 spatial transcriptomics techniques, such questions can now be addressed. Using multiplexed error-robust  
99 fluorescence in situ hybridization (MERFISH), an image-based method for spatially resolved single cell  
100 transcriptomics<sup>26,27</sup>, here we vividly decode the spatial organization of the PFC and its various  
101 subregions. Our results demonstrate distinct cellular composition of the PFC relative to its adjoining  
102 cortical areas. PFC adopts unique molecular features to suit its specific electrophysiological properties  
103 different from its adjacent motor cortex. We map molecular identities (and layer localization) of  
104 projection neurons to major subcortical targets. Finally, based on projection, transcription and activity  
105 marks, we reveal the molecular identity of PFC clusters most significantly affected in chronic pain.

106

107

108

109

110

111

112

113

114

115

116

117

118

119

120 **Results**

121

122 **MERFISH reveals molecular diversity and location of cell types in the frontal cortex**

123 To understand the diversity of cell types and determine their spatial organization within the PFC,  
124 we performed MERFISH<sup>26 27-29</sup>, the imaging-based method for single cell transcriptomics that uses  
125 combinatorial labeling of RNA species with error-robust barcoding which are read through iterative  
126 rounds of single-molecule FISH. MERFISH detects the precise location of each RNA molecule to  
127 ultimately reveal the spatial organization of diverse cell types within anatomically defined tissue regions  
128 (Fig. S1a)<sup>29 28</sup>. We constructed a MERFISH library to interrogate 416 genes consisting of cell-type  
129 markers and functionally important genes including- ion channels, neuropeptides, G-protein coupled  
130 receptors and a panel of neuronal activity regulated genes (Supplementary Table 1). We collected brain  
131 samples from three different mice and prepared rostral to caudal coronal slices covering +2.5 to +1.3  
132 from Bregma to broadly image the frontal cortex. Using established analysis pipelines<sup>29</sup>, imaged RNA  
133 species were detected, decoded and assigned to individual cells by segmentation based on poly(A) and  
134 nuclear (DAPI) staining (Fig. S1a). Overall, we obtained 487,224 high-quality cells in the frontal  
135 cortical region from three independent biological replicates with high consistency (Fig. S1b). Expression  
136 of individual genes showed good correlation with that of the bulk RNA-seq of the PFC (Fig. S1c).

137 After unsupervised clustering, we identified the major cell types including excitatory neurons,  
138 inhibitory neurons, and non-neuronal cells that include oligodendrocytes, oligodendrocyte precursors  
139 (OPC), microglia, endothelia, astrocytes and vascular leptomeningeal cells (VLMC) (Fig. 1a). Within  
140 the excitatory neurons, the major subgroups clustered together, as described by the commonly used  
141 nomenclature<sup>23</sup>: the intra-telencephalic (IT) populations of different layers, the extra-telencephalic (ET)  
142 neurons, the near projecting (NP) and the cortico-thalamic (CT) populations (Fig. 1a). Within the  
143 inhibitory neurons, populations from the medial ganglionic eminence (*Pvalb* and *Sst*) and the caudal  
144 ganglionic eminence (*Vip*, *Sncg* and *Lamp5*) clustered distinctly (Fig. 1a).

145 The major cell types were further clustered into 52 hierarchically organized cell subtypes,  
146 including 18 excitatory neuron subtypes, 19 inhibitory neuron subtypes, and 15 non-neuron subtypes  
147 (Fig. 1b). Among the excitatory IT neurons, four subtypes were detected in L2/3 (L2/3 IT 1 to 4), two  
148 subtypes in L4/5, three subtypes in L5, and two subtypes in L6. Additionally, the L5 ET split in two  
149 subtypes, the L6 CT into four subtypes and L5/6 NP formed a single cluster. Among the inhibitory  
150 neurons, the *Pvalb* and *Sst* each split into six subtypes, the *Lamp5* into three subtypes, the *Vip* and *Sncg*

151 into two subtypes each (Fig. 1b). Among the non-neurons, the endothelial cells formed five subtypes,  
152 Endo1-5, while astrocytes formed three subtypes, oligodendrocytes and OPCs each formed two  
153 subtypes.

154 Projecting these clusters in space (based on MERFISH coordinates) revealed the anatomical  
155 layout of the coronal section and depicted precise localization of every single cell (Fig. 1c; inset –  
156 magnified view showing individual cells). We found that molecularly similar excitatory neurons are  
157 localized together in space to form distinct layers, from which a laminar histology, characteristic of  
158 cerebral cortex, emerged (L2/3 IT to L6 CT: outside inwards) (Fig. 1c, left half). Within each layer, the  
159 subtypes are further organized in strata (e.g., L2/3 IT 1 to L2/3 IT 4) (Fig. 1c, right half: distribution of  
160 subtypes). Inhibitory neurons are broadly distributed and do not form specific layers, although some  
161 subtypes appear to be enriched within certain layers or subregions (Fig. 1c). Non-neuronal cells are also  
162 broadly distributed, except for enrichment of oligodendrocytes near the fiber tracts (e.g., corpus  
163 callosum) and the VLMC in the outermost layer of brain (Fig. 1c, yellow). As evidence of accurate  
164 localization, we mapped the RNA location of a few well-characterized genes that are known to express  
165 only in specific cortical layers. We found *Otof*, *Cux2* and *Fezf2* mRNAs are respectively localized to L2,  
166 L2/3 and L5 on the MERFISH slice, consistent with the ISH Images from Allen Brain Institute (Fig.  
167 S1d)

168 Together, excitatory neurons comprise the largest population in PFC, followed by non-neuronal  
169 cells combined and then the inhibitory neurons (Fig. 1d, left). Within excitatory, the IT neurons are the  
170 largest subgroup, followed by the ET, NP and CT of deeper layers, respectively (Fig. 1d, middle).  
171 Within the inhibitory, *Sst* and *Pvalb* neurons are most abundant followed by the *Lamp5*, *Scng* and *Vip*  
172 (Fig. 1d, right).

173 To further evaluate our detection accuracy, we first performed an integrated analysis of the  
174 MERFISH data with scRNA-seq data of the PFC from the Allen Institute<sup>23</sup>. All the major subtypes  
175 showed strong correlation between the two datasets (Fig. 1e). Similar integrated analysis comparing the  
176 MERFISH data with our own scRNA-seq of PFC<sup>19</sup> revealed strong correspondence even at the subtype  
177 levels (Fig. S2a-e, see Method). In fact, MERFISH could classify some of the scRNA-seq clusters at a  
178 finer resolution to reveal distinct subclusters (Fig. S2d, e). This point is particularly true for the  
179 inhibitory neurons (e.g. Inh 1, 2 and 7 of scRNA-seq), possibly due to their higher rate of detection in  
180 MERFISH (Fig. S2f).

181 Collectively, our results indicate that we have faithfully detected all known cell subtypes and  
182 their locations within the mouse frontal cortex, which enables us to analyze their spatial organization  
183 along all 3D axes within this region.

184

### 185 **Marked heterogeneity in spatial distribution of neuron subtypes along AP and DV axes in PFC**

186 To understand spatial organization of the different neuron subtypes within the anatomically  
187 defined PFC region, we aligned our profiled frontal cortex sections with the Allen Mouse Brain  
188 Common Coordinate Framework (CCFv3)<sup>30</sup>, a reference created for the mouse brain based on serial two  
189 photon tomography images of the 1675 C57Bl6/J mice (Fig. S3a), which outlines the PFC-boundaries  
190 within each section.

191 Mapping the MERFISH clusters onto the sequential antero-posterior sections revealed the order  
192 of cellular organization in 3D throughout the frontal cortex (Fig. 2a). Heterogeneous distribution of  
193 several neuron subtypes along the antero-posterior (A-P) and dorsal-ventral (D-V) axes was visually  
194 evident. Analysis along the AP axis revealed that L2/3 IT and L4/5 IT neuron subtypes are most  
195 enriched in the anterior-most part of the frontal cortex, where all types of L5 and L6 neurons are  
196 generally low (Fig. 2b). This density gradient follows a reverse order in posterior direction where deep  
197 layer neurons like L5 ET 1 or L6 CT 1-3 are gradually enriched (Fig. 2b). Detailed mapping of various  
198 neuron subtypes on the serial brain sections clearly revealed the uneven distribution along the A-P axis  
199 (Fig. 2c, S3b). In contrast, some subtypes such as L5/6 NP are modularly distributed and few others  
200 (e.g., L5 IT 2 or L6 IT 1) are sparse, but uniform throughout the A-P axis (Fig. 2b). IT neurons generally  
201 project to shorter distances within the telencephalon or cortex, while non-IT neurons predominantly  
202 project long distances outside telencephalon. This distribution likely favors the anterior bias of IT cells  
203 and the posterior bias of non-IT neurons closer to the subcortical region and the major fiber tracts.

204 There is also strong distribution heterogeneity among the inhibitory neurons, but it follows a  
205 pattern of regional enrichment instead of gradual transitions along the A-P axis (Fig. 2b). For some  
206 subtypes, such as Lamp5 3, Pvalb 4 and Vip 2, the fluctuation in density along the A-P axis is very  
207 prominent (Fig. 2b). Neighborhoods with high density of distinct interneuron subtypes may indicate  
208 regulatory hotspots and/or focal points for specific subcortical projections circuits. Such unique  
209 organization reaffirms the principle that function begets structure in biological systems. It is only  
210 through spatial transcriptomics that such information can be accurately revealed.

211 Another readily recognizable feature from the coronal slices is the laminar organization of  
212 various excitatory neurons along the DV axis, within each representative section (Fig. 2a). Computation  
213 of physical depth inward from the cortical surface revealed that IT neurons locate more superficially  
214 within each layer. The L2/3 IT (and L4/5 IT) subtypes are most superficial and closer to the surface of  
215 the brain (Fig. 2d). Similarly, in L5, most IT neurons (L5 IT 1, L5 IT 3) are superficial to the other  
216 populations of the layer (L5 ET 1, L5 ET 2) (Fig. 2d). Within Layer 6, although L6 IT 1 is superficial,  
217 L6 IT 2 mingles with the deepest CT subtypes (Fig. 2d). Plotting each population individually onto a  
218 representative coronal section, a highly specific spatial localization of each neuron subtypes in layers  
219 inwards from the surface is clearly resolved (Fig. 2f, S4a). This layered organization is precisely  
220 achieved during developmental migration of cortical neurons when the migrating wave of each cell type  
221 is regulated by cues originating from their final homing site/layer<sup>31</sup>. As such, the types and density of  
222 neurons can be influenced by local signals to form circuits or hotspots characteristic of distinct  
223 subregions. How such anatomic assemblies locally emerge, remains a matter of further study.

224 The DV organization of GABAergic interneurons was even more interesting. Although,  
225 inhibitory neurons, unlike the excitatory, are not organized in layers, most subtypes appear to be  
226 enriched within specific excitatory layers or subregions (Fig. 2e). Broadly, the Lamp5 (Lamp5 1 to 3)  
227 and Vip (Vip 1 and 2) neurons along with Sncg 1 are more enriched in superficial layers. Lamp5 3, for  
228 example, is restricted only to the superficial layer (Fig. 2e, f). However, Sncg 2 is broadly distributed  
229 along the entire depth (Fig. 2e, S4b). This appears to be different from neighboring motor cortex, as per  
230 recent reports<sup>32</sup>, where all subtypes of *Sncg* neurons are present only in superficial layers. Additionally,  
231 motor cortex also has some subtypes of *Vip* neurons in deeper layers, which was not detected in PFC.  
232 However, the most interesting observation is that specific molecular subtypes of Pvalb and Sst neurons  
233 are differentially enriched in various layers along the cortical depth (Fig. 2e). For example, while Pvalb  
234 5 and Pvalb 2 have higher density towards the superficial layers, Pvalb 3 and Pvalb 6 are enriched in the  
235 very deep layers, and Pvalb 1 and Pvalb 4 are maximally enriched in the intermediate region (Fig. 2e, 2f,  
236 S4b). Likewise, Sst 1 and Sst 5 are more superficially enriched, and the remaining are distributed in the  
237 intermediate to deep layers (Fig. 2e, S4b). Pvalb neurons can regulate excitatory pyramidal neuron firing  
238 through feedforward inhibition delivered directly onto the somatic compartment, while Sst neurons  
239 targets distal dendrites of excitatory neurons to impose feedback inhibition<sup>33,34</sup>. Although these  
240 interactions are indispensable to calibrate cortical excitatory output<sup>35</sup>, it is striking that inhibitory



241 neurons diversified distinct molecular subtypes to adapt to the molecular diversity of excitatory  
242 pyramidal neurons in each cortical layer.

243 Most non-neuronal subtypes displayed a more broad and dispersed distribution (Fig. S4c), with  
244 few exceptions. The vascular leptomeningeal cells (VLMC), for example, line the outermost surface  
245 along the cortex. The Oligo 1 and Oligo 2 are enriched near the regions of origin of the white matter  
246 tracts (Fig. S3c). The Astro 2 had significant presence in L1 and somewhat greater enrichment in the  
247 medial prefrontal region (Fig. S4c).

248

### 249 **Distinct neuron subtypes are uniquely enriched in PFC**

250 PFC is very distinct in function and connectivity compared to the adjacent cortices. We asked  
251 whether this functional and connectivity distinction is associated with its specialized cell composition.  
252 To this end, we identified the PFC boundary in each section by aligning with CCFv3 (Fig. S3a). By  
253 projecting the cells identified from the alignment as ‘in’-PFC onto the combined UMAP of frontal  
254 cortex (Fig. 3a), we found that some subtypes of excitatory neurons are selectively biased ‘in’, and some  
255 others ‘out’ of the defined PFC region (Fig. 3a), indicating different cellular composition in PFC and the  
256 adjacent areas. Relative population enrichment calculation showed that L2/3 IT 1, L5 ET 1 and L5 IT 1  
257 are about 8 folds enriched within the PFC, whereas L6 CT 2 and L6 CT 3 are enriched by more than 2  
258 folds (Fig. 3b). In contrast, L2/3 IT 4, L4/5 IT 1 or L6 IT 1 are markedly depleted (4-8 folds) in the PFC  
259 (Fig. 3b). When mapped onto the representative coronal section, the enriched, depleted and unbiased  
260 populations were clearly visible with respect to the boundaries of the PFC (Fig. 3c). Inhibitory neurons,  
261 although less abundant, exhibit clear subtype selectivity across all the major types in PFC (Fig. 3b).  
262 Switching of Pvalb subtypes (~2 fold enriched in Pvalb 3 and 4, and depleted in Pvalb 1, 2, and 6),  
263 depletion of Sncg 2 and enrichment of Sst 4 and 6, are the most prominent features (Fig. 3b, S5a). Also  
264 notably, Lamp5 3, the most superficially located interneuron (L1) is the only enriched Lamp5 neuron in  
265 PFC (Fig. 3b). The relative proportions of specific IT, ET and CT subtypes are intimately tied to the  
266 projections of a cortical area (inside and outside the telencephalon). The selection of specific  
267 interneurons determines the precise excitatory-inhibitory balance in the input/output circuits of the  
268 projections. In combination, these circuit motifs likely serve as a blueprint for the specialized functions  
269 of a cortical area, and PFC is clearly organized into a highly selective assembly in this regard.

270 The PFC has distinct functional subregions from its dorsal to ventral end, viz. anterior cingulate  
271 cortex (ACAd), prelimbic cortex (PL), infralimbic cortex (ILA) and dorso-peduncular cortex (DPP)

272 (Fig. 3d). We asked whether these subregions have distinct cellular composition. Indeed, clustering with  
273 the normalized cell proportions across all subregions revealed the most enriched excitatory neurons in  
274 each subregion (Fig. 3e). Projecting cell types on to a coronal slice with subregion demarcations  
275 revealed heterogeneity of subtype distribution across different subregions (Fig. 3f). For example, L5 ET  
276 1 is enriched in PL and ILA (but depleted in ACAd), while L6 CT 2 is mainly in ILA and L5 IT 3 is  
277 mainly in ACAd (Fig. 3e, f – enriched cells in 3e labeled red fonts). We also estimated the percent  
278 abundance of each cell type in each subregion (Fig. S5b). For example, L5 ET 1, L6 CT 2, L6 CT 3 or  
279 L6 CT 4 as well as inhibitory subtypes like Pvalb 5 or Sncg 2 are enriched in the infralimbic (ILA)  
280 relative to other subregions, while L2/3 IT 4, L4/5 IT 1, L5 IT 3 and especially L6 IT 1 are depleted in  
281 this subregion. Similarly, the dorsal anterior cingulate (ACAd) is enriched in L6 IT 1 or L2/3 IT 4, but  
282 depleted in L2/3 IT 1, L5 ET 2, L6 CT 2, L6 CT 3, L6 CT 4. Strikingly, the prelimbic (PL) maintains a  
283 steady share of cells from most subpopulations except for a higher percentage of L2/3 IT 2 and L4/5 IT  
284 2. It is well established that many behavioral functions are specifically regulated by distinct subregions  
285 of the PFC. For example, conditioned fear response or trauma (as evidenced in PTSD) is encoded in the  
286 ILA<sup>36</sup>, while cue or context-associated reward memory is encoded in PL<sup>37,38</sup>, and compulsive behavior  
287 (often associated with drug addiction) is associated with ORBm<sup>39</sup>. Thus, revealing the differential  
288 neuron subtype distribution in the different PFC subregions may help link the PFC subregion-specific  
289 functions to the various differentially distributed neuron subtypes.

290

### 291 **Unique transcriptional signatures emerge in PFC**

292 Functional differences across brain regions often underlie molecular adaptations<sup>23</sup>. The cortex is  
293 believed to be no exception. Thus, we asked whether the distinctive functions and cellular organization  
294 of the PFC is associated with specialized molecular features by comparing the transcriptome of PFC  
295 with that of the adjacent cortical regions. Indeed, a large number of genes interrogated in the MERFISH  
296 library are differentially expressed between the PFC and the neighboring cortices (Fig. 4a). Among the  
297 416 genes analyzed, 54 were significantly enriched and 40 depleted in PFC (adjusted p-Value <0.05;  
298 DEG >20%) (Supplementary Table S2). Mapping expression of significantly enriched (*Nnat*) or  
299 depleted (*Scn4b*) genes onto the coronal section showed clear enrichment or depletion in the PFC region  
300 (Fig. 4b), which is consistent with the ISH data from the Allen Brain Institute (Fig. 4c), validating our  
301 MERFISH results.

302 We next asked whether specific types or categories of genes are selectively enriched or depleted  
303 in PFC. The differentially expressed genes had a strong representation of several ion channels and some  
304 key neurotransmitter receptors- which can impart very distinct electrical properties of the PFC relative to  
305 adjoining cortices<sup>40</sup>. In the ion channels group, several potassium channels are enriched or depleted  
306 (Supplementary table 2). The voltage-gated potassium channels subtypes<sup>40-42</sup>, especially delayed  
307 rectifiers (*Kcna2*, *Kcnb2*, *Kcnc2*, *Kcnc3*, *Kcnq3*, *Kcnq5*) are depleted (Fig. 4a, Supplementary table 2).  
308 However, some other delayed rectifiers (e.g., *Kcna1*, *Kcna4*, *Kcna5*, etc.) are not changed  
309 (Supplementary table S2). On the other hand, the inward (*Kcnh7*) and outward (*Kcnh5*) rectifier  
310 channels are depleted (Fig. 4a). Additionally, enrichment of BK channel like *Kcnmb4*, and reciprocally  
311 enriched modifier/silencer *Kcng1* (up), *Kcnf1* (up) but *Kcnv1* (down), were also observed (Fig. 4a,  
312 Supplementary table S2) Interestingly, *Kcnn3* is upregulated, that controls neuronal firing through after-  
313 hyperpolarization and its mutation is implicated in schizophrenia and bipolar disorder<sup>43</sup>. Apart from  
314 potassium, some prominent calcium channels (*Cacna1e*, *Cacna1h*, Fig. S6a) and sodium (*Scn3b*)  
315 channels, which have been implicated in major neurological disorders like autism and epilepsy<sup>44-47</sup>, are  
316 also enriched.

317 Apart from gated ion channels, another striking observation is the selective enrichment of *Gria1*  
318 (Fig. 4a), a principal ionotropic AMPA glutamate receptor subunit, in PFC. A GluA1 (protein product of  
319 *Gria1* gene) dimer binds a GluA2 (from *Gria2* gene) dimer to form a tetrameric ionotropic glutamate  
320 receptor. The GluA1 is strongly implicated in several neuropsychiatric disorders (schizophrenia,  
321 epilepsy, depression), chronic pain (increase) and drug addiction (decrease)<sup>48</sup>. Its expression in PFC  
322 declines with age and GluA1 is also implicated in Alzheimer's disorder<sup>49</sup>. More interestingly, *Cacng8*, a  
323 transmembrane AMPA receptor-regulating auxiliary subunit, is also enriched within PFC (Fig. 4a). It  
324 regulates trafficking and gating of AMPA receptors and is implicated in several neuropsychiatric  
325 disorders (attention deficit or personality disorder)<sup>50,51</sup>. Enrichment of *Cxcl12* (Fig. 4a, S6a) is likely a  
326 final proof of the functional diversity of PFC. As a chemokine, *Cxcl12* plays roles from sculpting  
327 inhibitory neuron synapses to neuro-immune interactions, which in the adult cortex are characteristic of  
328 the PFC<sup>52-54</sup>.

329 To globally represent the remarkable transcriptional features of PFC neurons, we calculated the  
330 "PFC signature", the average expression of the top 10 enriched genes minus top 10 depleted genes.  
331 When values for this index were projected (as red color) onto cells in the original UMAP, the PFC-  
332 enriched excitatory neurons clearly clustered and emerged (Fig. 4d). When PFC signature was mapped

333 onto a representative coronal section, it localized precisely within the anatomical limits of the PFC (Fig.  
334 4e), indicating a distinct molecular composition of the PFC relative to the adjacent cortices.

335

### 336 **iSpatial revealed transcriptome-wide PFC-enriched genes and functional pathways**

337 To expand our spatial mapping of gene expression to the transcriptome scale, we next combined  
338 scRNA-seq with MERFISH to make predictions for spatial genes expression enrichment in PFC for  
339 genes not measured with MERFISH. To this end, we integrated our prior PFC scRNA-seq data<sup>19</sup> and  
340 current MERFISH data to predict the expression pattern of all genes using iSpatial<sup>55</sup>, a bioinformatic  
341 tool we developed. The analysis revealed 190 PFC-enriched and 182 PFC-depleted genes (Fig. 4f,  
342 Supplementary table S2). Mapping enriched and depleted candidate genes predicted by iSpatial, *Cdh13*  
343 and *Abcd2* respectively, on to a coronal section revealed consistent localization with respect to the PFC  
344 boundaries (Fig. S6b), which is in line with the Allen Brain ISH results (Fig. S6b).

345 Gene Ontology enrichment analysis of the 364 spatially differentially expressed genes revealed  
346 *biological function* categories highly enriched in transporters, channels and receptor activity, which are  
347 known to modulate membrane potential (Fig. 4g). Depletion of voltage-gated potassium channels or  
348 transmembrane potassium transporter concur with a poised state of activity that PFC neurons must  
349 maintain for working memory function, a feature not essential for adjacent motor or sensory cortices<sup>42,56</sup>.  
350 Greater enrichment of ‘postsynaptic neurotransmitter activity’ or ‘glutamate receptor activity’ (Fig. 4g)  
351 relative to adjacent cortices reaffirm that PFC retains significant plasticity compared to these regions,  
352 even in adult. Curiously, some functions like ‘gated channel’ or ‘cation channel activity’ are both  
353 enriched and depleted (Fig. 4g). This indicates that PFC likely uses a different subset of receptors (class  
354 switching) for the same functions compared to adjacent cortices to adapt to its distinct  
355 electrophysiological needs.

356 A signaling pathways enrichment analysis of these 364 genes revealed opioid signaling,  
357 endocannabinoid pathway and glutamate receptor signaling as the top three pathways (Fig. S6c). While  
358 glutamate signaling is widespread in cortex, opioid and cannabinoid signaling are more uniquely  
359 characteristic of the PFC and are known to be essential for normal physiological functions of mood,  
360 memory, feeding, etc.<sup>57-60</sup>. This indicates that the distinct molecular composition of PFC is indeed tied to  
361 its specialized functions.

362 Decoding the transcriptome-wide, spatially enriched, gene expression patterns also allowed us to  
363 investigate whether there is expression bias between subregions of the PFC. Indeed, we detected several

364 genes (e.g., *Nnat*, *Fezf2*, *Nr4a1*, and *Scn4b*, etc.) that are preferentially expressed in certain subregions  
365 of the PFC (Fig. 4h, S6d), which are also validated in Allen Brain ISH data (Fig. S6d). Thus, subregion-  
366 specific functions of PFC are potentially enabled by their discrete molecular compositions imparting  
367 specific electrical and signaling properties.

368

### 369 **Spatial organization predicts subtype-specific interactomes in PFC**

370 Extensive local processing of convergent and divergent signals is one of the principal  
371 characteristics of cortex and is particularly prominent in PFC, an area that integrates sensory/cognitive  
372 inputs in real time to govern executive function<sup>61</sup>. Integration of multilevel (thalamic, cortical or  
373 subcortical) inputs, their transfer through cortical layers, and modulation by interneuron inhibition as  
374 well as disinhibition all rely on extensive local interactions between neurons that are neighboring or  
375 located in close proximity within PFC<sup>34,62-64</sup>. Given that MERFISH allowed the mapping of the precise  
376 location of every cell in PFC, we explored the potential cell-cell interactions at the cell subtype level. To  
377 this end, we inspected the cell subtypes composition of the neighboring cells for each cell and calculated  
378 the enrichments of paired subtype-subtype colocalizations. Enrichment of proximity was notable  
379 amongst many groups of cells (Fig. S7a). IT subtypes of L2/3 are closely apposed in the superficial  
380 layers and engage in cortico-cortical interactions to integrate signals from sensory and association  
381 cortices (Fig. S7a). Interestingly, most of these subtypes have interactions with L4/5 IT subtypes (Fig.  
382 S7a) that receive exclusive inputs from thalamus or lower order cortex (since PFC has no clear L4), and  
383 are known to relay processed information mainly to L2/3<sup>65</sup>. This observation reinforces the notion that  
384 spatial organization of neuronal types reflect the order of information flow within the circuits they  
385 comprise, which in turn emerges as the systematic layered cortical structure. Interestingly, our analysis  
386 revealed specific interactions in the deeper layers that may not be apparent from histological  
387 organization alone. For example, L6 IT neurons (like L6 IT 1) share proximity with specific ET neurons  
388 (L5 ET 2), revealing subtype selectivity (and in turn circuit selectivity) within L5-L6 communication  
389 (Fig. S7a). Subtype selectivity is perhaps most important in excitatory-inhibitory coupling. The  
390 inhibitory *Pvalb* neurons directly access the soma of excitatory pyramidal neurons to regulate firing  
391 through feed forward inhibition<sup>66</sup>. Preferential pairing of many excitatory subtypes with one or few (but  
392 not all) specific *Pvalb* subtypes were detected in our analysis (Fig. S7a). For example, L5 IT 3 scored  
393 the highest proximity with *Pvalb* 1, while L5 ET 2 (located within the same layer) has greater interaction  
394 probability with *Pvalb* 6 (Fig. S6a- highlighted boxes). Mapping cells on to a representative coronal

395 section revealed the relative proximities of each of these two excitatory-inhibitory pairs, and also a  
396 different spatial enrichment of the Pvalb 1 and Pvalb 6 subtypes (Fig. S7b).

397 In summary, MERFISH measurements in the PFC allowed us to provide an entry point (or  
398 repository) for predicting subtype-specific synaptic interactions in the 3D anatomical space, which can  
399 be then studied by using appropriate experimental approaches.

400

### 401 **Spatial and molecular organization of PFC projection circuits to major subcortical targets**

402 It is well known that the PFC excitatory pyramidal neurons project to different subcortical targets  
403 including striatum, nucleus accumbens, thalamus, hypothalamus, amygdala, periaqueductal gray or  
404 ventral tegmental area<sup>18,67</sup>. However, the spatial organization and whether different neuron subtypes  
405 project to different targets are not well characterized.

406 A prior study has performed retrograde labeling and scRNA-seq for some of these major targets  
407 of labeled PFC neurons<sup>2</sup>. We integrated our PFC MERFISH data with this dataset to predict the PFC  
408 neuron subtypes with spatial/layer location projecting to these different targets. Through joint  
409 embedding and supervised machine learning, we could assign respective projection identity to the  
410 molecular clusters organized in space within the PFC (Fig. 5a). An overlap of the MERFISH and  
411 scRNA-seq clusters through UMAP visualization revealed a strong correspondence (Fig. 5b, S8a). The  
412 ROC curve for the prediction model independently predicted 6 different projection targets with high  
413 confidence, including contralateral PFC (cPFC), dorsal striatum (DS), hypothalamus (Hypo), nucleus  
414 accumbens (NAc), periaqueductal gray (PAG), and amygdala (Amyg) (Fig. 5c). Mapping these  
415 projection cells onto a coronal slice of frontal cortex revealed the identity and spatial organization of  
416 neurons that project to each of these 6 targets within the PFC (Fig. 5d). Distinct spatial localization of  
417 each of these 6 groups of cells can be visualized when mapped individually on the coronal slice (Fig.  
418 S8b). This analysis allowed us to associate different subsets of each neuronal type that project to  
419 different regions with their location within the brain (Fig. 5e), which reveals that most of the target brain  
420 regions receive projection from more than one neuron subtypes. For example, the amygdala receives  
421 projections from all four subtypes of L6 CT neurons as well L5 ET 1 neurons, but the majority comes  
422 from L6 CT 2. Likewise, the hypothalamus receives its projections from L5 ET 1 and L6 CT 1; dorsal  
423 striatum from L6 CT 1, 2, and 3; and NAc gets mainly from L6 CT 1, L5 ET 1 and some from L6 CT 2.  
424 However, one exception to the general rule is the PAG, which receives its projections almost exclusively  
425 from L5 ET, predominantly from L5 ET 1 (and some from L5 ET 2). Consistent with prior knowledge,

426 superficial layer IT neurons project to the contralateral hemisphere of PFC<sup>68</sup>. It should be noted that  
427 each of these target brain regions are involved in many different behavioral functions. For example,  
428 amygdala alone is implicated in fear, addiction, emotion, memory and pain<sup>69-71</sup>. It is expected that inputs  
429 will likely to be received from diverse projections (of different neuron subtypes) to selectively trigger  
430 specific synapses/pathways to sustain the functional complexity of PFC.

431 To validate our computational model-based neuron projection predication, we performed  
432 retrograde tracing from two of these target regions by injecting retrograde AAV virus into the PAG and  
433 the amygdala to drive mCherry expression. Four weeks after the injection, we prepared cryosections  
434 and performed single molecule FISH (RNAScope) to co-label mCherry RNA and the respective cell-  
435 type specific markers. Consistent with the prediction, all mCherry expressing PAG retro-traced PFC  
436 neurons exclusively colocalized with *Pou3f1*, a selective marker for L5 ET 1 and L5 ET 2 (Fig. 5f). In  
437 contrast, colocalization of mCherry was detected for both *Pou3f1* (L5 ET 1) and *Foxp2* (L6 CT) for  
438 amygdala as predicted (Fig. S8c). These data support the accuracy of our circuit predications.

439

#### 440 **Identifying PFC neuron subtypes involved in chronic pain**

441 Functions of PFC in cognition or execution are most widely studied. However, besides those  
442 voluntary behaviors, PFC also plays a pivotal role in autonomically modulating pain perception, and  
443 aberrations in this process is emerging as a major player in pain “chronification”<sup>5,14</sup>. While chronic pain  
444 is escalating as a leading healthcare challenge<sup>7</sup>, molecular underpinnings of the dysfunction remain  
445 unknown. Chronic pain has been strongly associated with transcriptional adaptations across the  
446 PFC<sup>5,72,73</sup>, the spatial or cell type-specific resolution of these changes are less clear. To explore the  
447 utility of our MERFISH datasets, we attempted to identify the PFC neuron subtypes involved in chronic  
448 pain by identifying the neuron subtypes that undergo the strongest transcriptional response in chronic  
449 pain.

450 To this end, we utilized the well-established spared nerve injury (SNI) model of chronic  
451 neuropathic pain in mice<sup>74</sup> where two of the three branches of the sciatic nerve are transected (Fig. 6a),  
452 which causes a state of chronic neuropathic pain in hind paw that lasts for months. Six weeks after  
453 surgery, brains from 3 pairs of sham and SNI mice were collected and characterized with MERFISH  
454 (Fig. 6a). Of all the neuronal subtypes, L5 ET 1 registered the strongest transcriptional response (with  
455 largest total number of differentially expressed genes), followed by the L6 CT 2 and L5 ET 2 (Fig. 6b).  
456 Lesser changes were detected in L6 CT 3, L5 IT 1, L6 IT 2, L2/3 IT 2 and L4/5 IT 2 (Fig. 6b). No

457 significant changes were detected in the other 30 clusters despite many of the excitatory neuron subtypes  
458 being highly abundant in PFC, suggesting these clusters are minimally affected in chronic pain.

459 Interestingly, the two highest impacted clusters respectively project to PAG (L5 ET 1) and amygdala  
460 (L6 CT 2) (Fig. 5e), the two major hotspots known to regulate sensory and affective aspects of pain<sup>5,71</sup>.

461 Chronic pain is known to inflict strong and sustained hypoactivity across the PFC<sup>9,12,14,75</sup>. We  
462 asked whether this can be detected in the baseline expression of neuronal activity-regulated genes  
463 (ARGs) to identify prominently affected neuron subtypes. We calculated ARG score using the mean  
464 expression of a panel of 5 ARGs (Arc, Junb, Fos, Npas4, Nr4a1) and compared between sham and SNI  
465 groups. We observed a strong and widespread reduction of ARG score when it is plotted on  
466 representative coronal sections (Fig. 6c). A subregion-specific calculation revealed that the ACAd and  
467 PL are the most impact PFC regions (Fig. 6d). We next compared the differences of ARG score across  
468 the individual excitatory neuron clusters (Fig. 6e), and found it is downregulated in several clusters,  
469 including those exhibiting transcriptional changes (e.g., L5 ET 1, L6 CT 3, Fig. 6b).

470 To validate chronic pain-induced hypoactivity across PFC, we performed single molecule FISH  
471 (smFISH) to compare Fos expression between sham and SNI brain sections. Although sham shows a  
472 baseline Fos activity in PFC, a general Fos depletion is obvious in the SNI (Fig. 6f). Co-staining Fos  
473 with Pou3f1, a selective marker for L5 ET1, revealed significant Fos depletion in this neuron subtype in  
474 the SNI brains (Fig. 6g, h).

475 Despite the conventional knowledge that a PFC-PAG circuit is involved in descending  
476 modulation of pain<sup>5</sup>, its cell type identity or changes in chronic pain were unclear. Our findings revealed  
477 the molecular identity and spatial organization of this circuit: the L5 ET 1 neurons with PAG projection  
478 (Fig. 5e), which are strongly deactivated in chronic pain (Fig. 6g) with the maximum transcriptional  
479 adaptation (Fig. 6b). Additionally, we also identified at least two CT subtypes in L6 (L6 CT 2 and 3)  
480 that project to limbic structures like amygdala, NAc and hypothalamus (Fig. 5e) that may be involved in  
481 the affective response to pain.

482



483 **Discussion**

484

485 In this study we present an account of how the PFC is distinctly organized at the cellular,  
486 molecular and projection levels relative to the adjacent regions within the frontal cortex. We exploit this  
487 characterization to reveal the molecular identity of key neuron subtypes that are engaged in chronic pain,  
488 and, more broadly, we provide a resource for the systematic mapping of functional ensembles and  
489 circuits selectively engaged in various cognitive and executive functions associated with PFC. Spatial  
490 transcriptomics is a rapidly growing field<sup>76</sup> and similar to recently reported brain regions<sup>29,32,77</sup>,  
491 MERFISH enabled a systematic decoding of PFC's cellular and molecular organization.

492

493 **The diversity of PFC neuron subtypes is consistent with its functional diversity**

494 We observed that there were a variety of neuronal subtypes largely specific to the PFC or to  
495 surrounding regions (Fig. 3a-c). Cellular composition of a cortical area should be predominantly  
496 governed by the input and output circuits associated with its function. This regional neuronal subtype  
497 specificity, in turn, may underlie the unique properties of the PCF relative to other cortical regions. For  
498 example, the PCF is agranular and lacks a typical L4, associated with thalamic input, it receives long-  
499 range inputs across all of its layers, and PFC neurons project to subcortical targets from almost all layers  
500 while PFC neurons engage in reciprocal connections with most of these functions<sup>78,79</sup>. Perhaps for the  
501 diverse functions, there is a 2-fold enrichment of the superficial-most IT neurons (L2/3 IT 1) to handle  
502 the cortico-cortical communications, but the subsequent IT populations (L2/3 IT 4 or L4/5 IT 1) are  
503 markedly depleted to make room for enrichment of L5 IT 1 or L5 ET 1 that engage in long distance  
504 subcortical projections. Enrichment of two CT subtypes (L6 CT 2 and 3) is consistent with the  
505 observation that CT neurons of PFC, unlike other cortices, project to several subcortical targets (Fig.  
506 5e), rather than thalamus alone. Notably, two of these enriched neuron subtypes (L5 ET 1 and L6 CT 2)  
507 eventually emerge as key subtypes engaged in chronic pain, a function exclusively performed by PFC  
508 (Fig. 6).

509 Depletion of certain subtypes of Pvalb (Pvalb 1, 2, 6), which also accounted for an overall lower  
510 count of Pvalb neurons in the PFC (relative to the adjacent regions), suggests that feedforward inhibition  
511 is differently organized in PFC. This either indicates an overall lower level of feed forward inhibition  
512 and perhaps a greater flexibility in excitatory-inhibitory balance; or larger receptive fields are covered  
513 by individual Pvalb neurons, synapsing with more pyramidal neurons towards a goal of regional

514 synchronization. In either case, this is an important observation as functional imbalance of Pvalb  
515 neurons has been implicated in almost every PFC-associated diseases, such as schizophrenia<sup>80</sup>, bipolar,  
516 depression, and chronic pain<sup>81</sup>. It should be noted that detection of such regional differences would not  
517 be possible without the spatial profiling techniques like MERFISH.

518 Besides cellular composition, we detected strong transcriptional features unique to the PFC. We  
519 found expression of a large number of ion channels and receptors is selectively increased or decreased in  
520 PFC relative to the adjacent cortical regions (Fig. 4). It is generally appreciated that different cortical  
521 regions have different baseline electrical properties and qualitatively different activity patterns, which in  
522 turn is critical for its specific function<sup>23</sup>. For example, sensory cortices, such as visual cortex, have  
523 millisecond scale dynamics which is believed to be much faster than that of frontal regions involved in  
524 decision, deliberation or short-term memory. Recording of electrical field potentials across cortical areas  
525 provide strong evidence supporting such regionally variable activity patterns<sup>82,83</sup>. However, the  
526 biological substrates underlying such functional differences have been less clear. Our findings revealing  
527 preferential expression or repression, or even subtype switch of a wide range of cation channels and key  
528 glutamate receptor subunits in PFC establish a foundation for identifying the potential biological  
529 substrates explaining the diverse PFC functions.

530

### 531 **The diverse projections of the PFC neuron subtypes**

532 As the apex controlling center for cognitive, executive and emotional behaviors, PFC has one of  
533 the most diverse efferent projection profiles amongst all cortical areas. However, a striking observation  
534 was that while targets like PAG receives projection from a more homogeneous molecular subtype in L5  
535 (L5 ET), most other brain regions receive heterogeneous projections from multiple cell types of different  
536 layers (Fig. 5). Although intriguing, this may in fact reflect a more sophisticated model of top-down  
537 control by PFC. Most of these target regions such as amygdala, striatum, nucleus accumbens, and  
538 hypothalamus engage in many different behavioral processes, which may also be regulated by distinct  
539 groups of neurons within each of these target regions. Accordingly, different lines of afferent projections  
540 from PFC can synapse on to different neuron populations to form separate circuits within a target and  
541 thereby separately modulate different behaviors under different contexts. Additionally, different  
542 subtypes in separate layers can receive distinct upstream inputs within PFC that can be separately  
543 relayed to the targets through specific projection clusters. For example, L5 ET1 and L6 CT2 may receive  
544 different upstream inputs in PFC and can also project to separate cell types within amygdala to modulate

545 different behaviors in separate contexts (Fig. 5e). Further work in this direction should reveal the  
546 cellular and molecular organization of all PFC projection circuits and identify specific ensembles  
547 engaged by different behaviors.

548

### 549 **The L5 ET1 neuron subtype might regulate chronic pain through PFC to PAG projection**

550 We identified the key cell types that are specifically impacted in PFC under chronic pain (Fig. 6).  
551 Amidst the rising prevalence of chronic pain and emerging consensus that transition to chronic pain is  
552 centrally regulated, there has been little clarity about the cellular and molecular mechanisms underlying  
553 the chronification, which is key to therapeutic targeting. Previous studies have shown that transcranial  
554 stimulation of PFC could relieve chronic pain<sup>15,84,85</sup>. Such studies, although established a causal  
555 connection, did not provide a long-term solution for pain management owing to the deleterious effects of  
556 broad non-specific cortex-wide stimulations. Despite a long-standing knowledge of putative PFC to  
557 PAG projections in descending inhibition of pain<sup>5</sup>, the molecular identity of this circuit was unknown. In  
558 this regard, our study revealing the L5 ET 1 as a major neuron subtype with exclusive projection to the  
559 PAG, and undergoes transcriptional changes under chronic pain state is of particular relevance. While it  
560 is likely that deactivation of this cluster will impair descending inhibition of pain which paves way for  
561 persistent pain/sensitivity, it remains to be determined if it also contributes to the affective component of  
562 pain. However, L6 CT 2 and L6 CT 3, the two other implicated clusters, project to multiple limbic  
563 regions including amygdala, NAc and hypothalamus, and their dysfunctions may elicit strong negative  
564 effect characteristic of chronic pain states<sup>71,86,87</sup>. All these remain valuable prospects for future  
565 functional studies through targeted neuronal activity manipulation using genetically engineered animal  
566 models.

567

568

569 **Materials and methods**

570

571 **Mice and Surgery**

572 All experiments were conducted in accordance with the National Institute of Health Guide for  
573 Care and Use of Laboratory Animals and approved by the Institutional Animal Care and Use Committee  
574 (IACUC) of Boston Children's Hospital and Harvard Medical School. Wildtype male C57BL6 mice of  
575 about 10 weeks old were used for the study. Mice were maintained at 12h light/dark cycles with food  
576 and water ad libitum. For the spared nerve injury surgery, mice were anesthetized with ketamine. Hair  
577 was shaved above the knee on one side (usually left) and the skin was sterilized with iodine and  
578 isopropanol. The muscles were separated by blunt dissection to expose all three branches of the sciatic  
579 nerve. The tibial and common peroneal branches of the nerve that run parallel were tied tightly with two  
580 sutures and a piece between the two ties was transected and removed. Care was taken that the third  
581 branch (sural nerve) was untouched during the whole procedure. The retracted muscles were released,  
582 and the skin stitched back. In the sham surgery group, identical steps were followed to expose the nerve,  
583 but no transection was performed, and skin was stitched back in position. Mice tissues were harvested 6  
584 weeks after the surgery.

585

586 **MERFISH Encoding Probes**

587 A library of MERFISH encoding probes for all target genes was generated as described  
588 previously<sup>29</sup>. Briefly, a unique binary barcode was assigned to each gene based on an encoding scheme  
589 with 24-bits, a minimum Hamming distance of 4 between all barcodes, and a constant Hamming weight  
590 of 4. This barcoding scheme left 60 'blank' barcodes unused to serve as a measure of false-positive  
591 rates. For each gene, 50 to 70 30-nt-long targeting regions with limited homology to other genes and  
592 narrow melting temperature and GC ranges were selected, and individual encoding probes to that gene  
593 were created by concatenating two 20-nt-long readout sequences to each of these target regions. Each of  
594 the 24 bits were associated with a unique readout sequences, and encoding probes for a given gene  
595 contained only readout sequences for which the associated bit in the barcode assigned to that gene  
596 contained a '1'. Template molecules to allow the production of these encoding probes were designed by  
597 adding flanking PCR primers, with one primer representing the T7 promoter. This template oligopool  
598 was synthesized by Twist Biosciences and enzymatically amplified to produce encoding probes using  
599 published protocols<sup>29</sup>.

600

601 **MERFISH tissue processing and imaging**

602 Tissue was prepared for MERFISH as described previously<sup>29</sup>. Briefly, mice were euthanized under CO<sub>2</sub>  
603 and brains were quickly harvested and rinsed with ice-cold calcium and magnesium free PBS. The  
604 brains were frozen on dry ice and stored at -80 °C till sectioning. The frozen brains were embedded in  
605 OCT on a mixture of ethanol and dry ice. Serial 14-µm-thick sections of the frontal cortex spaced about  
606 150 µm apart were collected and placed on poly-D lysine coated, silanized coverslips, containing orange  
607 fiducial beads, prepared as described previously<sup>29</sup>. The sections were allowed to briefly air dry and  
608 immediately fixed with 4% PFA for 10 mins. Sections were washed in PBS and stored in 70% ethanol  
609 for at least 12h to permeabilize. The sections were washed in hybridization buffer (2xSSC+30%  
610 formamide) and then drained and inverted over parafilm in petri dish onto a 50 µl droplet of mixture  
611 containing encoding probes and a poly(A) anchor probe<sup>29</sup> in hybridization buffer (2xSSC, 30%  
612 formamide, 0.1% yeast tRNA, 10% dextran sulfate) and hybridized in a covered humid incubator at  
613 37°C for 2 days. Coverslips were then washed in hybridization buffer and the sections were embedded  
614 into a thin film of poly-acrylamide gel, as described previously. The embedded sections were then  
615 digested for 2 days in a 2xSSC buffer containing 2% SDS, 0.5% Triton X-100 and 1:100 proteinase K.  
616 The coverslips were washed and stored in 2xSSC at 4 °C until imaging. MERFISH imaging was  
617 performed on a custom microscope and flow system, as described previously<sup>29</sup>. In each imaging round,  
618 the volume of each slice was imaged by collecting a z-stack at each field-of-view containing 10 images  
619 each spaced by 1 micron. 12 imaging rounds using two readout probes per imaging round were used to  
620 read out the 24-bit barcodes. Readout probes were synthesized by Biosynthesis and contained either a  
621 Cy5 or Alexa750 conjugated to the oligonucleotide probe via a disulfide bond, which allowed reductive  
622 cleavage to remove fluorophores after imaging, as described previously. A readout conjugated to  
623 Alexa488 and complementary to a readout sequence contained on the polyA anchor probe was  
624 hybridized with readouts associated with the first two bits in the first round of imaging.

625

626 **Image processing, decoding and cell segmentation**

627 MERFISH data was decoded as previously described<sup>29</sup>. Briefly, images of fiducial beads  
628 collected for each field-of-view in each imaging round were used to align images across imaging rounds.  
629 RNAs were detected using a pixel-based approach, in which images were first high-pass filtered,  
630 deconvolved, and low-pass filtered. Differences in the brightness of different imaging rounds were

631 corrected by an optimized set of scaling values, determined from an iterative process of decoding  
632 performed on a randomly selected subset of fields-of-view, and the intensity trace for individual pixels  
633 across all imaging rounds was matched to the barcode with the closest predicted trace as judged via a  
634 Euclidean metric and subject to a minimum distance. Adjacent pixels matched to the same barcode were  
635 aggregated to form putative RNAs. RNA molecules were then filtered based on the number of pixels  
636 associated with each molecule (greater than 1) and their brightness to remove background.

637 As described previously<sup>29</sup>, the identification of cell boundaries within each FOV was performed  
638 by a seeded watershed approaching using DAPI images as the seeds, and the poly(A) signals to identify  
639 segmentation boundaries. Following segmentation, individual RNA molecules were assigned to specific  
640 cells based on localization within the segmented boundaries.

641

### 642 **Preprocessing of MERFISH data**

643 The decoded data was preprocessed by the following steps: 1) Segmented “cells” with a cell  
644 body volume less than  $100 \mu\text{m}^3$  or larger than 4000 were removed; 2) Cells with total RNA counts of  
645 less than 10 or higher than 98% quantile, and cells with total RNA features less than 10, were removed;  
646 3) To correct for the minor batch fluctuations in different MERFISH experiments, we normalized the  
647 total RNA counts per cell to a same value (500 in this case); 4) Doublets were removed by Scrublet<sup>88</sup>; 5)  
648 The processed cell-by-gene matrix was transferred to gene-by-cell matrix and then loaded into Seurat  
649 V4<sup>89</sup> for downstream analysis. The matrix was log-transformed by the Seurat standard pipeline.

650

### 651 **Cell clustering**

652 Two rounds of cell clustering were used to identify cell types and subtypes. In the first round, we  
653 identified the three major cell types: excitatory neurons, inhibitory neurons, and non-neuronal cells. In  
654 the second round, each major cell type was further clustered. Excitatory neuron was further clustered  
655 into 18 subtypes, inhibitory neurons was further clustered into 19 subtypes, non-neuronal cell was  
656 further clustered into 15 subtypes. Then, we separated the excitatory subtypes into seven groups  
657 according to the neuronal projection: L2/3 IT, L4/5 IT, L5 IT, L6 IT, L5 ET, L5/6 NP, and L6 CT. The  
658 inhibitory neuron was cataloged into five groups based on the main markers: Lamp5, Pvalb, Sncg, Sst,  
659 and Vip. Non-neuronal cells were cataloged into six groups: endothelial cells, microglia,  
660 oligodendrocytes, OPC, astrocytes, and VLMC. Each round of clustering following the same workflow  
661 as described previously. First, all gene expression was centered and scaled via a z-score, and PCA was

662 applied on the scaled matrix. To determine the number of principal components (PCs) to keep, we used  
663 the same method described before<sup>29,77</sup>. Briefly, the scaled matrix was randomly shuffled and PCA was  
664 performed based on the shuffled matrix. This shuffling step was repeated 10 times and the mean  
665 eigenvalue of the first principal component crossing the 10 iterations was calculated. Only the principal  
666 components derived from the original matrix that had an eigenvalue greater than the mean eigenvalue  
667 were kept. Harmony<sup>90</sup> was then used to remove apparent batch effect among different MERFISH  
668 samples. The corrected PCs were used for cell clustering. The nearest neighbors for each cell were then  
669 computed by a K-nearest neighbor (KNN) graph in corrected PC space. Bootstrapping was used for  
670 determining the optimal k value for KNN as previously described<sup>29,77</sup> (k = 10 in the first round  
671 clustering. k = 50, 20, 15 for excitatory neurons, inhibitory neurons, and non-neuronal cells in the  
672 second round). Leiden method was used for detecting clusters<sup>91</sup>. The resolution was set to 0.3 in the first  
673 round clustering, and to 2 for the second round. Finally, we manually removed the clusters representing  
674 doublets, which express high levels of the established markers of multiple cell types. Clusters located  
675 outside of the cortex were also removed.

### 676

### 677 **Correspondence between scRNA-seq and MERFISH clusters**

678 To compare the cell clusters identified by scRNA-seq and MERFISH, we first co-embedded the  
679 two datasets in a corrected PCA space using Harmony as described above. Then, all the cells from both  
680 scRNA-seq and MERFISH were used to build the KNN graph. The first 30 corrected PCs were inputted  
681 into Seurat::FindNeighbors to compute the KNN. For each cell cluster in MERFISH, we obtained the  
682 cell cluster's nearest 30 neighbor cells' information. Then, we calculated the percentages of the cell  
683 clusters derived from scRNA-seq that were near to this MERFISH cluster, from which we obtained a  
684 correspondence matrix, where each row is a cluster from scRNA-seq, each column is a cluster from  
685 MERFISH, the element in the matrix indicates the similarity between the two clusters. Similarly, for  
686 each cell cluster in scRNA-seq, we inquired the nearest clusters derived from MERFISH data to  
687 generate another correspondent matrix. The average of the two correspondent matrices were used to  
688 indicate the similarities between the cell clusters defined by scRNA-seq and MERFISH.

### 689

### 690 **Cell-cell proximity**

691 For each cell, we first identified the nearest 30 neighbors based on spatial distance. Next, we  
692 derived the cell subtypes of these neighboring cells, and obtained the cell subtypes composition of these

693 cells nearby the inquired cell. After iteration of all cells in all subtypes, we could calculate the number of  
694 occurrences of paired cell-cell and obtain the cell-cell proximity matrix (Observed matrix). Because of  
695 the cell number differences for each subtype, we normalized cell-cell proximity matrix by a random  
696 shuffled matrix (Expected matrix). To derive the shuffled matrix, we first shuffled the cell identities by  
697 random assign a subtype for each cell. Then, the random cell-cell proximity matrix was calculated by the  
698 same method before. Finally, the normalized cell-cell proximity matrix was calculated by  $\log_2(\text{Observed}$   
699  $\text{matrix}/\text{Expected matrix})$ . In addition, the p-values were calculated by wilcoxon rank tests (using  
700 `wilcox.test` in R) and then adjusted by Benjamini-Hochberg method (using `p.adjust` in R, `method =`  
701 `"BH"`).

702

### 703 **Excitatory neuron projection prediction**

704 The scRNA-seq data (GEO: GSE161936)<sup>2</sup> was first preprocessed by standard Seurat pipeline.  
705 Only the cells from dorsomedial (dmPFC) and ventromedial (vmPFC) regions were used. We integrated  
706 the MERFISH and scRNA-seq data using Harmony, and all the cells derived from MERFISH/scRNA-  
707 seq were co-embedded on a corrected PCA space. The first corrected 30 PCs were selected as features to  
708 train a multi-class support vector machine (SVM) for predicting the neuronal projection. The cells from  
709 scRNA-seq were separated into training and test groups. Then, the SVM was trained on training data  
710 and validated on test data by using the radial basis function kernel. Gamma was set to 0.01, cost was set  
711 to 10. The receiver operating characteristic (ROC) curve was plotted to evaluate the performance using  
712 `pROC` package in R and the area under the AUC curve (AUC) was equal to 0.913. Finally, the model  
713 was applied to MERFISH cells to predict their projections.

714

### 715 **Register MERFISH slice to Allen Brain Atlas**

716 To align MERFISH slices to the Allen common coordinate framework (CCF) v3 we leveraged  
717 the spatial distribution of cells identified by MERFISH in each slice as well as DAPI images of that  
718 slice. First, each brain slice was paired to the closest matching coronal section in CCF v3 with the help  
719 of DAPI image and spatial location of the cell types. Then, we modified the `WholeBrain` package<sup>92</sup> to  
720 align the MERFISH slice to the corresponding matching CCF coronal section. To assure accurate  
721 alignment, we leveraged the MERFISH cell typing result at single cell resolution and used certain cell  
722 types as anchors to help locating the anatomic features. VLMC cells are used for marking the surface of  
723 brain slice as follows: Inhibitory neuron subtype, `Lamp5 3`, for locating layer 1; `L2/3 IT` neurons for



724 locating layer 2, L6 CT neurons for locating layer 6, oligodendrocytes for locating corpus callosum.  
725 Since some small slices do not have sufficient features to align, 45 out of 60 slices are successfully  
726 registered to CCF v3, which allowed us to define the anatomic PFC and PFC subregions.

727

### 728 **Differentially expressed genes between pain and control conditions**

729 To detect differentially expressed genes (DEGs) and correct the batch effects, we used a logistic  
730 regression framework. For each gene, we constructed a logistic regression model to predict the sample  
731 conditions  $C$  by considering the batch information  $S$ ,  $C \sim E + S$ , and compared with a null model,  
732  $C \sim 1 + S$ , with a likelihood ratio test. Then, Bonferroni correction method was applied to adjust for  
733 multiple comparisons. Here, “LR” method in Seurat FindAllMarkers was used for conducting this  
734 analysis.

735

### 736 **Data and code availability**

737 The MERFISH data generated in this study has been deposited to Brain Image Library with  
738 accession number: **in the process of uploading**. Interactive visualization of MERFISH data can be  
739 accessed at: <https://yizhang-lab.github.io/PFC>. Code for MERFISH analysis is available at  
740 <https://github.com/YiZhang-lab/PFC-MERFISH>.

741

742 **Acknowledgements**

743 We thank Drs. Barbara Calderone and Olga Alekseenko from the Harvard Neurobehavior Core  
744 for their support; Dr. Renchao Chen for critical reading of the manuscript and valuable suggestions; Drs.  
745 Yingying Zhang, Yuanyou Wang and Paolo Cadinu, and Ms. Rosalind Xu for help with MERFISH  
746 troubleshooting and pipelines. This project was supported by the National Institutes of Health  
747 (1R01DA042283, 1R01DA050589), the Open Philanthropy Foundation, and the HHMI. Y.Z. is an  
748 investigator of the Howard Hughes Medical Institute. This article is subject to HHMI's Open Access to  
749 Publications policy. HHMI lab heads have previously granted a nonexclusive CC BY 4.0 license to the  
750 public and a sublicensable license to HHMI in their research articles. Pursuant to those licenses, the  
751 author-accepted manuscript of this article can be made freely available under a CC BY 4.0 license  
752 immediately upon publication.

753

754 **Author Contributions**

755 Y.Z. conceived the project; A.B., Y.Z., and J.R.M. designed experiments; Y.Z. and J.R.M.  
756 supervised the project; A.B. performed experiments; C.Z. analyzed the data; M.N.D helped with probe  
757 design; B.W. built the MERFISH microscope and trained A.B. for MERFISH experiments; A.B., C.Z.,  
758 Y.Z. and J.R.M. interpreted the data and wrote the manuscript.

759

760 **Competing Interests**

761 J.R.M. is a co-founder of and consultant for Vizgen. The remaining authors declare no  
762 competing interests.

763

764 **Figure legends**

765

766 **Fig. 1: MERFISH reveals the molecularly diverse cell types and subtypes comprising the PFC.** **a**,  
767 UMAP visualization of all cells identified by MERFISH. Cells are colored coded by their identities. **b**,  
768 Dendrogram showing the hierarchical relationship among all molecular defined cell subtypes. The  
769 expression of marker genes is shown below. The color represents the average expression, and dot size  
770 indicates the percentage of cells expressing each gene. **c**, Spatial map of all cell subtypes in a  
771 represented coronal slice. An enlarged view of a zoom-in region is shown in the top-right. **d**, Pie charts  
772 showing the cell proportions of the major cell types (left), excitatory neurons (middle) and inhibitory  
773 neurons (right) in PFC. **e**, Heatmap showing the gene-expression correlation between cell types and  
774 subtypes defined by MERFISH and scRNA-seq. scRNA-seq data are downloaded from Allen brain  
775 atlas, and only cells from PFC are used.

776

777 **Fig. 2: Spatial organization of different neuron subtypes in PFC.** **a**, Coronal MERFISH slices  
778 showing the spatial organization of neuron subtypes from anterior to posterior in PFC and adjacent  
779 regions. The dotted lines indicate the PFC region. The color scheme is the same as in Fig. 1c. **b**,  
780 Heatmap showing the proportions of neuron subtypes within PFC from anterior to posterior (A to P)  
781 sections in excitatory (left) and inhibitory (right) neurons. **c**, Spatial organization of L4/5 IT 1 and L5  
782 ET 1 from anterior to posterior sections. **d**, **e**, Violin plots showing the cortical depth distributions of  
783 excitatory neuron subtypes (**d**) and inhibitory neuron subtypes (**e**) in PFC. The maximum cortical depth  
784 is normalized to 1. **f**, Spatial location of five representative neuron subtypes (excitatory neuron subtypes:  
785 L2/3 IT 2, L5 ET 1 L5/6 NP; and inhibitory neuron subtypes: Lamp5 3, Pvalb 3) on a coronal slice. Red  
786 dots mark the indicated cell types and gray dots mark the other cells.

787

788 **Fig. 3: Distinct neuron subtypes are uniquely enriched or depleted in PFC relative to the adjacent**  
789 **cortical regions.** **a**, UMAP of all MERFISH cells colored by their spatial location whether in or out of  
790 PFC. **b**, Barplot showing the log<sub>2</sub> of the abundance ratio of subtype neurons in or out of PFC. **c**, Spatial  
791 location of excitatory neuron subtypes enriched (left), depleted (middle), and unbiased (right)  
792 distribution in PFC compare with adjacent regions. Dotted line marks PFC in the slice. **d**, Diagram of  
793 anatomical subregions of PFC and adjacent cortical regions. **e**, The normalized neuron proportion of  
794 excitatory subtypes in different anatomical subregions. **f**, Spatial location of four representative

795 excitatory neuron subtypes on a coronal slice. Red dots represent the indicated subtypes. The dotted  
796 lines indicate the anatomical subregions from Allen Brain Atlas CCF v3.

797

798 **Fig. 4: Genes with expression enriched or depleted in PFC.** **a**, Volcano plot showing the  
799 differentially expressed genes (DEGs) that are enriched or depleted in PFC neurons relative to the  
800 neurons out of PFC. Expression of genes enriched, depleted in PFC are colored in red, blue dots,  
801 respectively. **b**, Spatial gene expression of *Nnat* (top) and *Scn4b* (bottom) in all excitatory neurons.  
802 Dotted line marks PFC region. **c**, *In situ* hybridization (ISH) data from Allen Brain Atlas showing the  
803 spatial expression of *Nnat* and *Scn4b* in a coronal slice (right) with zoom-in (left). **d**, UMAP of all  
804 MERFISH cells (bottom-left) and excitatory neurons colored by the PFC signature, which is defined as  
805 the average expression of top 10 enriched genes minus the average expression of top 10 depleted genes.  
806 **e**, Align the PFC signature onto a representative slice to show the spatial distribution of PFC signature. **f**,  
807 Volcano plot showing the expressions of genes enriched or depleted in PFC after imputing by iSpatial.  
808 A total 20,733 genes are analyzed. Genes analyzed by MERFISH are colored in black, and genes  
809 inferred by iSpatial are colored in yellow. **g**, The gene ontology enrichment analysis of genes that  
810 enriched or depleted in PFC. **h**, Gene expression enrichment analysis of genes enriched in the different  
811 anatomical subregions of PFC and the adjacent cortical regions.

812

813 **Fig. 5: Spatial and molecular organization of PFC excitatory subtypes projection to the major**  
814 **PFC targets.** **a**, Schematics of the strategy for inferring neuronal projection of MERFISH clusters. The  
815 MERFISH and scRNA-seq data are integrated into a reduced dimensional space. A support vector  
816 machine is used to predict neuronal projection of the MERFISH neuron subtypes (see methods). **b**,  
817 UMAP visualization of cells derived from MERFISH and scRNA-seq data after integration. **c**, The ROC  
818 curves showing the prediction powers of six projection targets. w/o represents the cells without  
819 projection information. **d**, A coronal slice showing *in silico* retrograde tracing from six injection sites,  
820 labeled by different colors as indicated. **e**, The inferred projection targets of molecularly defined  
821 excitatory neuron subtypes, represented by an alluvial diagram. **f**, PFC to PAG projection validation.  
822 Retrograde mCherry expressing AAV was injected in PAG and brain slice of PFC was used for  
823 smFISH. mCherry (red) labeled neurons co-express the L5 ET1 marker *Pou3f1* (green). All mCherry  
824 positive neurons are *Pou3f1*-positive.

825

826

827 **Fig. 6: Chronic pain caused cellular and molecular changes in PFC excitatory neurons. a,**

828 Overview of chronic pain sample preparation. For each MERFISH run, one brain slice from each of  
829 control and pain condition are loaded together to avoid batch effect. Seven paired samples from three  
830 paired mice were imaged. **b,** The numbers of differentially expressed genes comparing pain and control  
831 samples for the indicated neuron subtypes are shown. The numbers of up-regulated and down-regulated  
832 genes are colored in red and blue, respectively. **c,** Spatial distribution of cells colored by activity-  
833 regulated genes (ARG) scores in control and pain conditions. The anatomical subregions of PFC are also  
834 shown. **d,** Heatmap showing ARG score in PFC subregions in pain and control samples. **e,** ARG scores  
835 of PFC excitatory subtypes in pain and control samples. Paired dots represent the control-pain paired  
836 samples which were imaged together. Color of the paired dots represent the paired mice ID. Two-tailed  
837 paired t-test is used to calculate the p-value. **f,** Global overview of PFC in half coronal section with Fos  
838 smFISH (red) in Sham (Control) and chronic pain conditions. **g,** smFISH co-labeling of Fos and Pou3f1  
839 (L5 ET marker) at high magnification in Sham and chronic pain conditions. Arrowheads in merged  
840 images indicate double positive neurons. **h,** Barplot showing the percentage of cFos+ cells to Pou3f1+  
841 cells. Nine random fields are surveyed. Two-tailed Mann-Whitney test is used to calculate the p-value.

842

843

844

845

846

847 **Supplementary figure legends**

848

849 **Fig. S1: The workflow and quality control for MERFISH profiling.** **a**, The workflow of MERFISH  
850 profiling of mouse PFC, including MERFISH imaging, decoding, segmentation and data analysis. **b**,  
851 Scatterplot showing the spearman correlation of the RNA counts per cell of individual genes measured  
852 by MERFISH in two independent experiments. **c**, Scatterplot of the RNA counts per cell of individual  
853 genes measured by MERFISH versus bulk RNA-seq data. The counts are natural logarithms. **d**, Spatial  
854 gene expression of three representative genes detected by MERFISH. *In situ* hybridization (ISH) data  
855 from Allen Brain Atlas are shown at the bottom.

856

857 **Fig. S2: MERFISH and scRNA-seq based clusters are consistent.** **a**, UMAP showing integration of  
858 cells from MERFISH or scRNA-seq data (GSE124952). **b**, UMAP showing the cell clusters defined by  
859 scRNA-seq (left) or MERFISH (right). **c,d,e**, Heatmap showing the correspondence between main cell  
860 types (**c**), excitatory (**d**) and inhibitory (**e**) subtypes defined by MERFISH and scRNA-seq. **f**, The cell  
861 proportions of the excitatory, inhibitory and non-neuronal cells from scRNA-seq or MERFISH.

862

863 **Fig. S3: Spatial distribution of molecularly defined excitatory neuron subtypes along the anterior**  
864 **to posterior axis.** **a**, Schematics of coronal brain slices aligned to Allen Brain Atlas CCF-v3 from  
865 anterior to posterior sections. **b**, Spatial organization of the indicated representative excitatory neuron  
866 subtypes across anterior to posterior sections.

867

868 **Fig. S4: Spatial location of all molecularly defined PFC cell types and subtypes.**

869 **a**, Excitatory neuron subtypes; **b**, Inhibitory neuron subtypes; **c**, non-neuron cell types and subtypes. Red  
870 dots represent the indicated cell types and subtypes.

871

872 **Fig. S5: Distinct neuron subtypes are uniquely enriched in PFC and PFC subregions.** **a**, Spatial  
873 location of three enriched (top panels: Pvalb 1, Pvalb 2, and Pvalb 6) and three depleted (bottom panels:  
874 Pvalb 3, Pvalb 4, and Sst 6) inhibitory subtypes on a coronal slice. **b**, The proportion of cell numbers  
875 from different PFC subregions and adjacent cortical regions of all neuron and non-neuron subtypes.

876

877 **Fig. S6: Specific gene expression signatures of PFC and PFC subregions. a,b**, Spatial expression of  
878 two representative genes enriched (a) and depleted (b) in PFC relative to adjacent cortical regions. Only  
879 excitatory neurons are shown. Corresponding ISH data from Allen Brain Atlas are shown on the right.  
880 Dotted line marks PFC region. c, Ingenuity pathway analysis (IPA) of the genes, identified after  
881 imputation, showing enriched or depleted in PFC. The red/blue bars indicate the pathway more active  
882 in/out PFC, respectively. d, Spatial gene expression of four representative genes enriched in PFC  
883 subregions. A diagram of anatomical subregions in PFC and adjacent regions is shown on the left. Only  
884 the excitatory neurons are shown. ISH data from Allen Brain Atlas are shown on the right. Dotted line  
885 marks PFC subregion.

886

887 **Fig. S7: Cell-Cell proximity across all cell types. a**, Enrichment of cell-cell proximity between  
888 different cell types and subtypes shown in dot plot. The color represents log<sub>2</sub> transformed observation to  
889 expectation of co-localized frequency of two clusters. The size of dots indicates the significance of the  
890 co-localization. b, The cell-cell proximity between Pvalb 1 and L5 IT 3 neurons (left), and between  
891 Pvalb 6 and L5 ET 2 neurons (right).

892

893 **Fig. S8: Integrate MERFISH and scRNA-seq data to predict neuronal projections. a**, UMAP  
894 showing integration of cells from scRNA-seq (left) and MERFISH (right). The colors represent the  
895 projection sites in scRNA-seq data and the excitatory subtype in MERFISH data, respectively. b, Spatial  
896 location of neurons projecting to six different brain regions. c, Amygdala projection validation: mCherry  
897 expressing retrograde AAV was injected in amygdala. Brain slice of PFC were stained with DAPI and  
898 mCherry to image the labeled neurons. smFISH co-labeling of mCherry with *Pou3f1* (L5 ET marker), or  
899 *Foxp2* (L6 CT marker) reveal partial overlap with both neuron subtypes.

900

901

902 **List of Supplemental Tables**

903

904 **Table S1: List of MERFISH probes**

905 **Table S2: List of enriched and depleted genes in PFC compared to the adjacent cortical regions**

906 **Table S3: List of genes whose expression is affected by chronic pain**

907

908 **References**

909

- 910 1 Miller, E. K. & Cohen, J. D. An integrative theory of prefrontal cortex function. *Annu Rev Neurosci* **24**,  
911 167-202 (2001). <https://doi.org/10.1146/annurev.neuro.24.1.167>
- 912 2 Lui, J. H. *et al.* Differential encoding in prefrontal cortex projection neuron classes across cognitive tasks.  
913 *Cell* **184**, 489-506 e426 (2021). <https://doi.org/10.1016/j.cell.2020.11.046>
- 914 3 Gamo, N. J. & Arnsten, A. F. Molecular modulation of prefrontal cortex: rational development of  
915 treatments for psychiatric disorders. *Behav Neurosci* **125**, 282-296 (2011).  
916 <https://doi.org/10.1037/a0023165>
- 917 4 Chini, M. & Hanganu-Opatz, I. L. Prefrontal Cortex Development in Health and Disease: Lessons from  
918 Rodents and Humans. *Trends Neurosci* **44**, 227-240 (2021). <https://doi.org/10.1016/j.tins.2020.10.017>
- 919 5 Tan, L. L. & Kuner, R. Neocortical circuits in pain and pain relief. *Nat Rev Neurosci* **22**, 458-471 (2021).  
920 <https://doi.org/10.1038/s41583-021-00468-2>
- 921 6 Bushnell, M. C., Ceko, M. & Low, L. A. Cognitive and emotional control of pain and its disruption in  
922 chronic pain. *Nat Rev Neurosci* **14**, 502-511 (2013). <https://doi.org/10.1038/nrn3516>
- 923 7 Yong, R. J., Mullins, P. M. & Bhattacharyya, N. Prevalence of chronic pain among adults in the United  
924 States. *Pain* **163**, e328-e332 (2022). <https://doi.org/10.1097/j.pain.0000000000002291>
- 925 8 Gaskin, D. J. & Richard, P. The economic costs of pain in the United States. *J Pain* **13**, 715-724 (2012).  
926 <https://doi.org/10.1016/j.jpain.2012.03.009>
- 927 9 Zhou, H. *et al.* A novel neuromodulation strategy to enhance the prefrontal control to treat pain. *Mol*  
928 *Pain* **15**, 1744806919845739 (2019). <https://doi.org/10.1177/1744806919845739>
- 929 10 Deer, T. R. *et al.* The appropriate use of neurostimulation: new and evolving neurostimulation therapies  
930 and applicable treatment for chronic pain and selected disease states. Neuromodulation  
931 Appropriateness Consensus Committee. *Neuromodulation* **17**, 599-615; discussion 615 (2014).  
932 <https://doi.org/10.1111/ner.12204>
- 933 11 Baliki, M. N., Geha, P. Y., Apkarian, A. V. & Chialvo, D. R. Beyond feeling: chronic pain hurts the brain,  
934 disrupting the default-mode network dynamics. *J Neurosci* **28**, 1398-1403 (2008).  
935 <https://doi.org/10.1523/JNEUROSCI.4123-07.2008>
- 936 12 Davis, K. D. & Moayed, M. Central mechanisms of pain revealed through functional and structural MRI. *J*  
937 *Neuroimmune Pharmacol* **8**, 518-534 (2013). <https://doi.org/10.1007/s11481-012-9386-8>
- 938 13 Nardone, R. *et al.* rTMS of the prefrontal cortex has analgesic effects on neuropathic pain in subjects  
939 with spinal cord injury. *Spinal Cord* **55**, 20-25 (2017). <https://doi.org/10.1038/sc.2016.87>
- 940 14 Jefferson, T., Kelly, C. J. & Martina, M. Differential Rearrangement of Excitatory Inputs to the Medial  
941 Prefrontal Cortex in Chronic Pain Models. *Front Neural Circuits* **15**, 791043 (2021).  
942 <https://doi.org/10.3389/fncir.2021.791043>
- 943 15 Li, C. *et al.* Prolonged Continuous Theta Burst Stimulation Can Regulate Sensitivity on Abeta Fibers: An  
944 Functional Near-Infrared Spectroscopy Study. *Front Mol Neurosci* **15**, 887426 (2022).  
945 <https://doi.org/10.3389/fnmol.2022.887426>
- 946 16 Ong, W. Y., Stohler, C. S. & Herr, D. R. Role of the Prefrontal Cortex in Pain Processing. *Mol Neurobiol* **56**,  
947 1137-1166 (2019). <https://doi.org/10.1007/s12035-018-1130-9>
- 948 17 Ossipov, M. H., Morimura, K. & Porreca, F. Descending pain modulation and chronification of pain. *Curr*  
949 *Opin Support Palliat Care* **8**, 143-151 (2014). <https://doi.org/10.1097/SPC.0000000000000055>
- 950 18 Anastasiades, P. G. & Carter, A. G. Circuit organization of the rodent medial prefrontal cortex. *Trends*  
951 *Neurosci* **44**, 550-563 (2021). <https://doi.org/10.1016/j.tins.2021.03.006>
- 952 19 Bhattacharjee, A. *et al.* Cell type-specific transcriptional programs in mouse prefrontal cortex during  
953 adolescence and addiction. *Nat Commun* **10**, 4169 (2019). <https://doi.org/10.1038/s41467-019-12054-3>

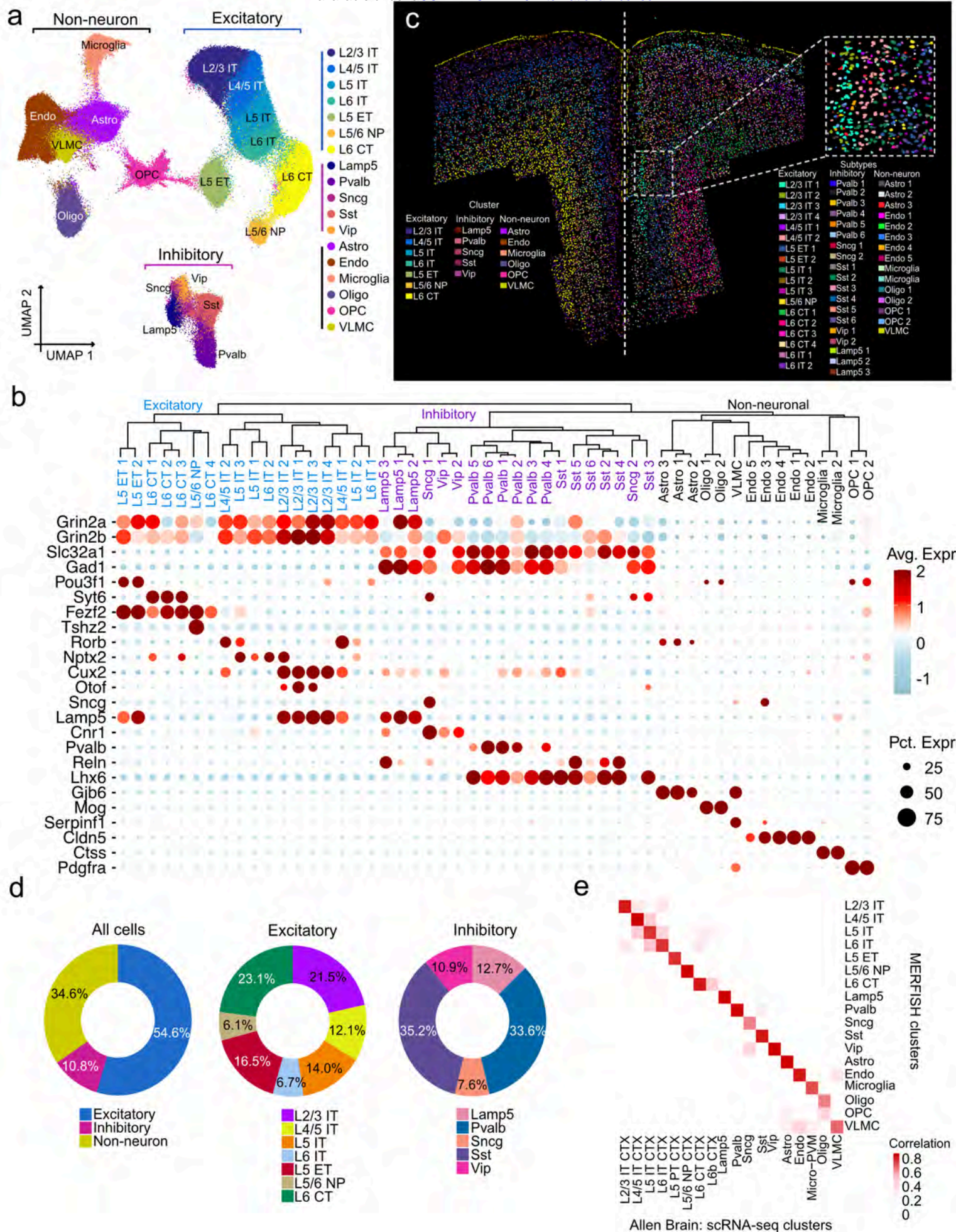


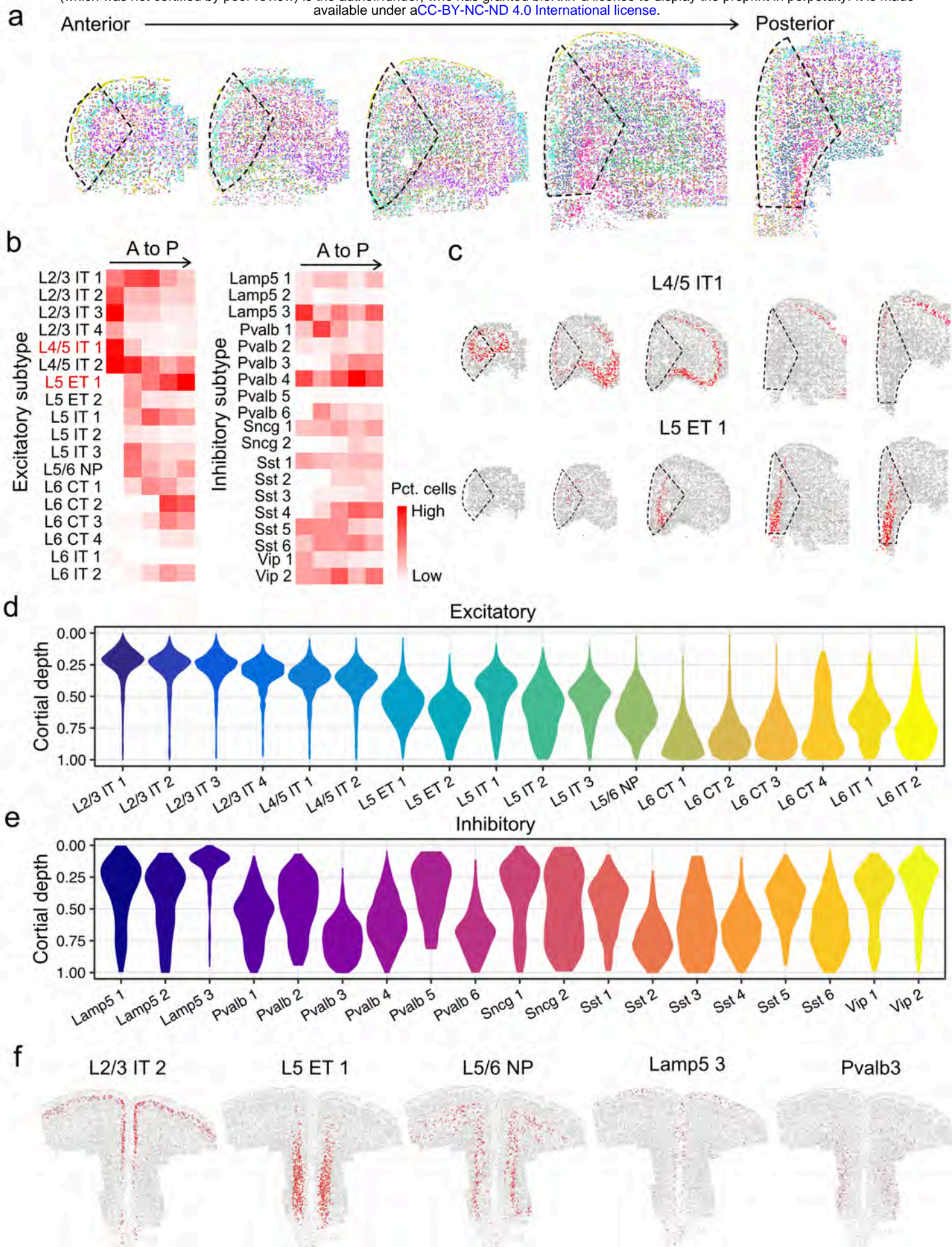
- 954 20 Zeng, H. & Sanes, J. R. Neuronal cell-type classification: challenges, opportunities and the path forward. *Nat Rev Neurosci* **18**, 530-546 (2017). <https://doi.org/10.1038/nrn.2017.85>
- 955 21 Network, B. I. C. C. A multimodal cell census and atlas of the mammalian primary motor cortex. *Nature*
- 956 **598**, 86-102 (2021). <https://doi.org/10.1038/s41586-021-03950-0>
- 957 22 Radnikow, G. & Feldmeyer, D. Layer- and Cell Type-Specific Modulation of Excitatory Neuronal Activity in
- 958 the Neocortex. *Front Neuroanat* **12**, 1 (2018). <https://doi.org/10.3389/fnana.2018.00001>
- 959 23 Tasic, B. *et al.* Shared and distinct transcriptomic cell types across neocortical areas. *Nature* **563**, 72-78
- 960 (2018). <https://doi.org/10.1038/s41586-018-0654-5>
- 961 24 Loo, L. *et al.* Single-cell transcriptomic analysis of mouse neocortical development. *Nat Commun* **10**, 134
- 962 (2019). <https://doi.org/10.1038/s41467-018-08079-9>
- 963 25 Li, Y. E. *et al.* An atlas of gene regulatory elements in adult mouse cerebrum. *Nature* **598**, 129-136
- 964 (2021). <https://doi.org/10.1038/s41586-021-03604-1>
- 965 26 Chen, K. H., Boettiger, A. N., Moffitt, J. R., Wang, S. & Zhuang, X. RNA imaging. Spatially resolved, highly
- 966 multiplexed RNA profiling in single cells. *Science* **348**, aaa6090 (2015).
- 967 <https://doi.org/10.1126/science.aaa6090>
- 968 27 Xia, C., Fan, J., Emanuel, G., Hao, J. & Zhuang, X. Spatial transcriptome profiling by MERFISH reveals
- 969 subcellular RNA compartmentalization and cell cycle-dependent gene expression. *Proc Natl Acad Sci U S*
- 970 *A* **116**, 19490-19499 (2019). <https://doi.org/10.1073/pnas.1912459116>
- 971 28 Moffitt, J. R. & Zhuang, X. RNA Imaging with Multiplexed Error-Robust Fluorescence In Situ Hybridization
- 972 (MERFISH). *Methods Enzymol* **572**, 1-49 (2016). <https://doi.org/10.1016/bs.mie.2016.03.020>
- 973 29 Moffitt, J. R. *et al.* Molecular, spatial, and functional single-cell profiling of the hypothalamic preoptic
- 974 region. *Science* **362** (2018). <https://doi.org/10.1126/science.aau5324>
- 975 30 Wang, Q. *et al.* The Allen Mouse Brain Common Coordinate Framework: A 3D Reference Atlas. *Cell* **181**,
- 976 936-953 e920 (2020). <https://doi.org/10.1016/j.cell.2020.04.007>
- 977 31 Oishi, K. *et al.* Identity of neocortical layer 4 neurons is specified through correct positioning into the
- 978 cortex. *Elife* **5** (2016). <https://doi.org/10.7554/eLife.10907>
- 979 32 Zhang, M. *et al.* Spatially resolved cell atlas of the mouse primary motor cortex by MERFISH. *Nature* **598**,
- 980 137-143 (2021). <https://doi.org/10.1038/s41586-021-03705-x>
- 981 33 Isaacson, J. S. & Scanziani, M. How inhibition shapes cortical activity. *Neuron* **72**, 231-243 (2011).
- 982 <https://doi.org/10.1016/j.neuron.2011.09.027>
- 983 34 Jang, H. J. *et al.* Distinct roles of parvalbumin and somatostatin interneurons in gating the
- 984 synchronization of spike times in the neocortex. *Sci Adv* **6**, eaay5333 (2020).
- 985 <https://doi.org/10.1126/sciadv.aay5333>
- 986 35 Brown, J. A. *et al.* Inhibition of parvalbumin-expressing interneurons results in complex behavioral
- 987 changes. *Mol Psychiatry* **20**, 1499-1507 (2015). <https://doi.org/10.1038/mp.2014.192>
- 988 36 Santini, E., Quirk, G. J. & Porter, J. T. Fear conditioning and extinction differentially modify the intrinsic
- 989 excitability of infralimbic neurons. *J Neurosci* **28**, 4028-4036 (2008).
- 990 <https://doi.org/10.1523/JNEUROSCI.2623-07.2008>
- 991 37 Otis, J. M. *et al.* Prefrontal cortex output circuits guide reward seeking through divergent cue encoding.
- 992 *Nature* **543**, 103-107 (2017). <https://doi.org/10.1038/nature21376>
- 993 38 Spring, M. G., Soni, K. R., Wheeler, D. S. & Wheeler, R. A. Prelimbic prefrontal cortical encoding of
- 994 reward predictive cues. *Synapse* **75**, e22202 (2021). <https://doi.org/10.1002/syn.22202>
- 995 39 Harada, M., Pascoli, V., Hiver, A., Flakowski, J. & Luscher, C. Corticostriatal Activity Driving Compulsive
- 996 Reward Seeking. *Biol Psychiatry* **90**, 808-818 (2021). <https://doi.org/10.1016/j.biopsych.2021.08.018>
- 997 40 Humphries, E. S. & Dart, C. Neuronal and Cardiovascular Potassium Channels as Therapeutic Drug
- 998 Targets: Promise and Pitfalls. *J Biomol Screen* **20**, 1055-1073 (2015).
- 999 <https://doi.org/10.1177/1087057115601677>
- 1000

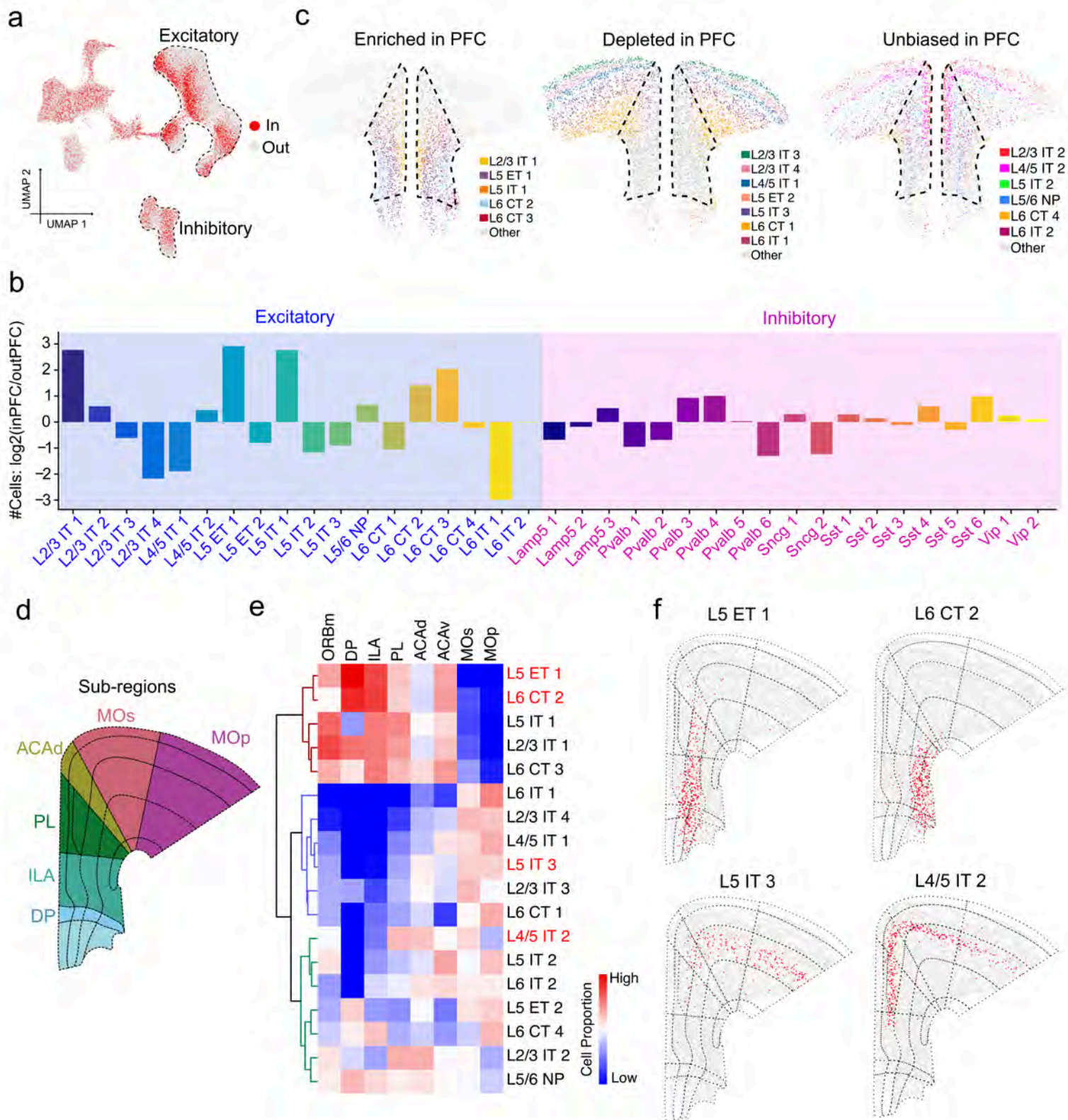
- 1001 41 Gonzalez Sabater, V., Rigby, M. & Burrone, J. Voltage-Gated Potassium Channels Ensure Action Potential  
1002 Shape Fidelity in Distal Axons. *J Neurosci* **41**, 5372-5385 (2021).  
1003 <https://doi.org/10.1523/JNEUROSCI.2765-20.2021>
- 1004 42 Lai, H. C. & Jan, L. Y. The distribution and targeting of neuronal voltage-gated ion channels. *Nat Rev*  
1005 *Neurosci* **7**, 548-562 (2006). <https://doi.org/10.1038/nrn1938>
- 1006 43 Grube, S. *et al.* A CAG repeat polymorphism of KCNN3 predicts SK3 channel function and cognitive  
1007 performance in schizophrenia. *EMBO Mol Med* **3**, 309-319 (2011).  
1008 <https://doi.org/10.1002/emmm.201100135>
- 1009 44 Andrade, A. *et al.* Genetic Associations between Voltage-Gated Calcium Channels and Psychiatric  
1010 Disorders. *Int J Mol Sci* **20** (2019). <https://doi.org/10.3390/ijms20143537>
- 1011 45 Eckle, V. S. *et al.* Mechanisms by which a CACNA1H mutation in epilepsy patients increases seizure  
1012 susceptibility. *J Physiol* **592**, 795-809 (2014). <https://doi.org/10.1113/jphysiol.2013.264176>
- 1013 46 Carvill, G. L. Calcium Channel Dysfunction in Epilepsy: Gain of CACNA1E. *Epilepsy Curr* **19**, 199-201  
1014 (2019). <https://doi.org/10.1177/1535759719845324>
- 1015 47 Splawski, I. *et al.* CACNA1H mutations in autism spectrum disorders. *J Biol Chem* **281**, 22085-22091  
1016 (2006). <https://doi.org/10.1074/jbc.M603316200>
- 1017 48 Zhang, J. & Abdullah, J. M. The role of GluA1 in central nervous system disorders. *Rev Neurosci* **24**, 499-  
1018 505 (2013). <https://doi.org/10.1515/revneuro-2013-0021>
- 1019 49 Qu, W. *et al.* Emerging role of AMPA receptor subunit GluA1 in synaptic plasticity: Implications for  
1020 Alzheimer's disease. *Cell Prolif* **54**, e12959 (2021). <https://doi.org/10.1111/cpr.12959>
- 1021 50 Forrest, M. P., Parnell, E. & Penzes, P. Dendritic structural plasticity and neuropsychiatric disease. *Nat*  
1022 *Rev Neurosci* **19**, 215-234 (2018). <https://doi.org/10.1038/nrn.2018.16>
- 1023 51 Peng, S. X. *et al.* SNP rs10420324 in the AMPA receptor auxiliary subunit TARP gamma-8 regulates the  
1024 susceptibility to antisocial personality disorder. *Sci Rep* **11**, 11997 (2021).  
1025 <https://doi.org/10.1038/s41598-021-91415-9>
- 1026 52 Festa, L. K. *et al.* CXCL12-induced rescue of cortical dendritic spines and cognitive flexibility. *Elife* **9**  
1027 (2020). <https://doi.org/10.7554/eLife.49717>
- 1028 53 Wu, P. R., Cho, K. K. A., Vogt, D., Sohal, V. S. & Rubenstein, J. L. R. The Cytokine CXCL12 Promotes Basket  
1029 Interneuron Inhibitory Synapses in the Medial Prefrontal Cortex. *Cereb Cortex* **27**, 4303-4313 (2017).  
1030 <https://doi.org/10.1093/cercor/bhw230>
- 1031 54 Sanfilippo, C., Castrogiovanni, P., Imbesi, R., Nunnari, G. & Di Rosa, M. Postsynaptic damage and  
1032 microglial activation in AD patients could be linked CXCR4/CXCL12 expression levels. *Brain Res* **1749**,  
1033 147127 (2020). <https://doi.org/10.1016/j.brainres.2020.147127>
- 1034 55 Zhang, C., Chen, R. & Zhang, Y. Accurate inference of genome-wide spatial expression with iSpatial. *Sci*  
1035 *Adv* **8**, eabq0990 (2022). <https://doi.org/10.1126/sciadv.abq0990>
- 1036 56 Kurowski, P., Grzelka, K. & Szulczyk, P. Ionic Mechanism Underlying Rebound Depolarization in Medial  
1037 Prefrontal Cortex Pyramidal Neurons. *Front Cell Neurosci* **12**, 93 (2018).  
1038 <https://doi.org/10.3389/fncel.2018.00093>
- 1039 57 Selleck, R. A. *et al.* Endogenous Opioid Signaling in the Medial Prefrontal Cortex is Required for the  
1040 Expression of Hunger-Induced Impulsive Action. *Neuropsychopharmacology* **40**, 2464-2474 (2015).  
1041 <https://doi.org/10.1038/npp.2015.97>
- 1042 58 Baldo, B. A. Prefrontal Cortical Opioids and Dysregulated Motivation: A Network Hypothesis. *Trends*  
1043 *Neurosci* **39**, 366-377 (2016). <https://doi.org/10.1016/j.tins.2016.03.004>
- 1044 59 Tan, H., Ahmad, T., Loureiro, M., Zunder, J. & Laviolette, S. R. The role of cannabinoid transmission in  
1045 emotional memory formation: implications for addiction and schizophrenia. *Front Psychiatry* **5**, 73  
1046 (2014). <https://doi.org/10.3389/fpsy.2014.00073>

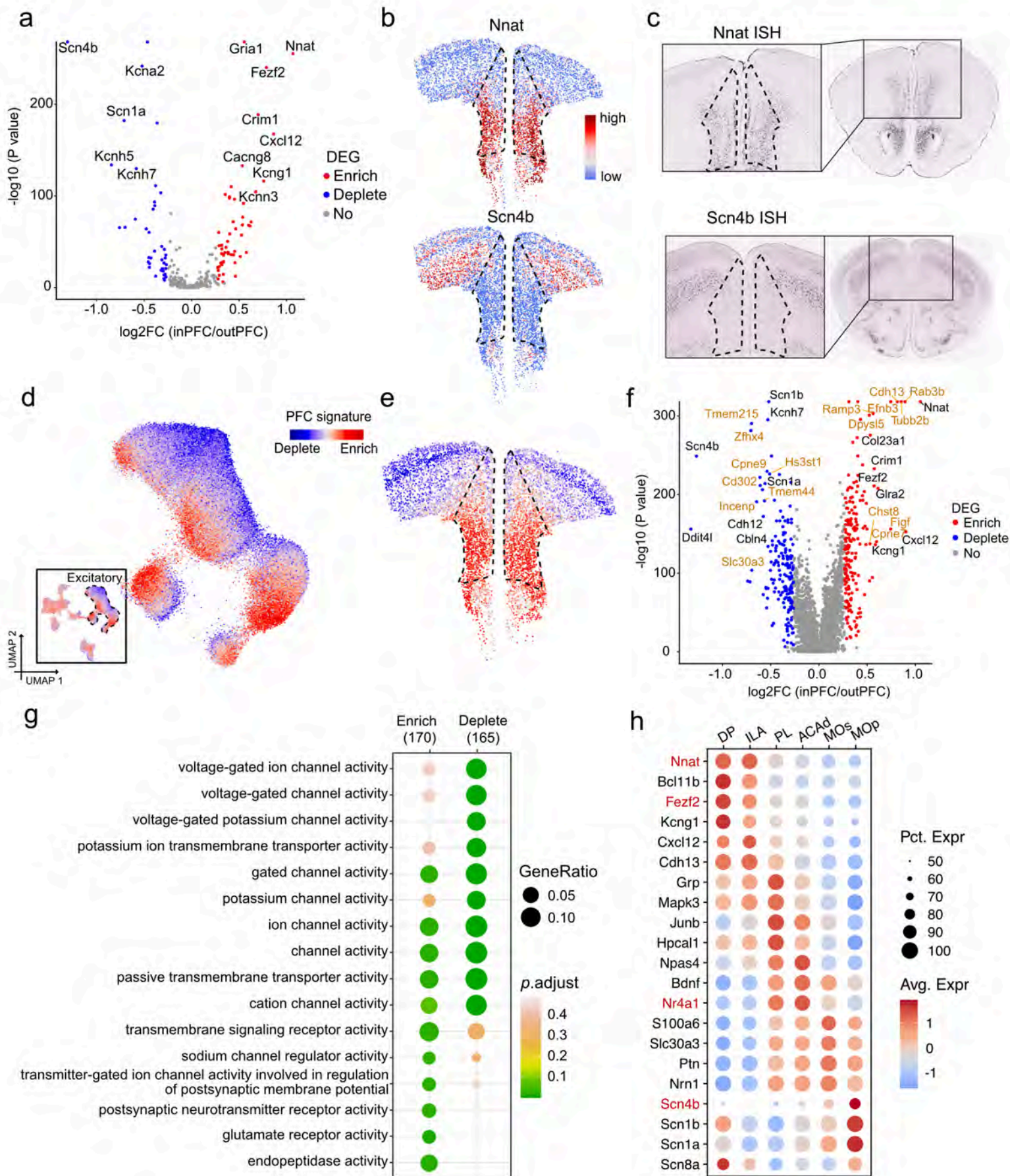
- 1047 60 Egerton, A., Allison, C., Brett, R. R. & Pratt, J. A. Cannabinoids and prefrontal cortical function: insights  
1048 from preclinical studies. *Neurosci Biobehav Rev* **30**, 680-695 (2006).  
1049 <https://doi.org/10.1016/j.neubiorev.2005.12.002>
- 1050 61 Peron, S. *et al.* Recurrent interactions in local cortical circuits. *Nature* **579**, 256-259 (2020).  
1051 <https://doi.org/10.1038/s41586-020-2062-x>
- 1052 62 LaBerge, D. & Kasevich, R. S. Neuroelectric Tuning of Cortical Oscillations by Apical Dendrites in Loop  
1053 Circuits. *Front Syst Neurosci* **11**, 37 (2017). <https://doi.org/10.3389/fnsys.2017.00037>
- 1054 63 Lacefield, C. O., Pnevmatikakis, E. A., Paninski, L. & Bruno, R. M. Reinforcement Learning Recruits  
1055 Somata and Apical Dendrites across Layers of Primary Sensory Cortex. *Cell Rep* **26**, 2000-2008 e2002  
1056 (2019). <https://doi.org/10.1016/j.celrep.2019.01.093>
- 1057 64 Karimi, A., Odenthal, J., Drawitsch, F., Boergens, K. M. & Helmstaedter, M. Cell-type specific innervation  
1058 of cortical pyramidal cells at their apical dendrites. *Elife* **9** (2020). <https://doi.org/10.7554/eLife.46876>
- 1059 65 Harris, K. D. & Shepherd, G. M. The neocortical circuit: themes and variations. *Nat Neurosci* **18**, 170-181  
1060 (2015). <https://doi.org/10.1038/nn.3917>
- 1061 66 Wamsley, B. & Fishell, G. Genetic and activity-dependent mechanisms underlying interneuron diversity.  
1062 *Nat Rev Neurosci* **18**, 299-309 (2017). <https://doi.org/10.1038/nrn.2017.30>
- 1063 67 Gabbott, P. L., Warner, T. A., Jays, P. R., Salway, P. & Busby, S. J. Prefrontal cortex in the rat: projections  
1064 to subcortical autonomic, motor, and limbic centers. *J Comp Neurol* **492**, 145-177 (2005).  
1065 <https://doi.org/10.1002/cne.20738>
- 1066 68 Zingg, B. *et al.* Neural networks of the mouse neocortex. *Cell* **156**, 1096-1111 (2014).  
1067 <https://doi.org/10.1016/j.cell.2014.02.023>
- 1068 69 Baxter, M. G. & Croxson, P. L. Facing the role of the amygdala in emotional information processing. *Proc*  
1069 *Natl Acad Sci U S A* **109**, 21180-21181 (2012). <https://doi.org/10.1073/pnas.1219167110>
- 1070 70 Bonnet, L. *et al.* The role of the amygdala in the perception of positive emotions: an "intensity detector".  
1071 *Front Behav Neurosci* **9**, 178 (2015). <https://doi.org/10.3389/fnbeh.2015.00178>
- 1072 71 Corder, G. *et al.* An amygdalar neural ensemble that encodes the unpleasantness of pain. *Science* **363**,  
1073 276-281 (2019). <https://doi.org/10.1126/science.aap8586>
- 1074 72 Topham, L. *et al.* The transition from acute to chronic pain: dynamic epigenetic reprogramming of the  
1075 mouse prefrontal cortex up to 1 year after nerve injury. *Pain* **161**, 2394-2409 (2020).  
1076 <https://doi.org/10.1097/j.pain.0000000000001917>
- 1077 73 Descalzi, G. *et al.* Neuropathic pain promotes adaptive changes in gene expression in brain networks  
1078 involved in stress and depression. *Sci Signal* **10** (2017). <https://doi.org/10.1126/scisignal.aaj1549>
- 1079 74 Richner, M., Bjerrum, O. J., Nykjaer, A. & Vaegter, C. B. The spared nerve injury (SNI) model of induced  
1080 mechanical allodynia in mice. *J Vis Exp* (2011). <https://doi.org/10.3791/3092>
- 1081 75 Denk, F., McMahon, S. B. & Tracey, I. Pain vulnerability: a neurobiological perspective. *Nat Neurosci* **17**,  
1082 192-200 (2014). <https://doi.org/10.1038/nn.3628>
- 1083 76 Moffitt, J. R., Lundberg, E. & Heyn, H. The emerging landscape of spatial profiling technologies. *Nat Rev*  
1084 *Genet* **23**, 741-759 (2022). <https://doi.org/10.1038/s41576-022-00515-3>
- 1085 77 Chen, R. *et al.* Decoding molecular and cellular heterogeneity of mouse nucleus accumbens. *Nat*  
1086 *Neurosci* **24**, 1757-1771 (2021). <https://doi.org/10.1038/s41593-021-00938-x>
- 1087 78 Collins, D. P., Anastasiades, P. G., Marlin, J. J. & Carter, A. G. Reciprocal Circuits Linking the Prefrontal  
1088 Cortex with Dorsal and Ventral Thalamic Nuclei. *Neuron* **98**, 366-379 e364 (2018).  
1089 <https://doi.org/10.1016/j.neuron.2018.03.024>
- 1090 79 Song, C. & Moyer, J. R., Jr. Layer- and subregion-specific differences in the neurophysiological properties  
1091 of rat medial prefrontal cortex pyramidal neurons. *J Neurophysiol* **119**, 177-191 (2018).  
1092 <https://doi.org/10.1152/jn.00146.2017>

- 1093 80 Lodge, D. J., Behrens, M. M. & Grace, A. A. A loss of parvalbumin-containing interneurons is associated  
1094 with diminished oscillatory activity in an animal model of schizophrenia. *J Neurosci* **29**, 2344-2354  
1095 (2009). <https://doi.org/10.1523/JNEUROSCI.5419-08.2009>
- 1096 81 Zhang, Z. *et al.* Role of Prelimbic GABAergic Circuits in Sensory and Emotional Aspects of Neuropathic  
1097 Pain. *Cell Rep* **12**, 752-759 (2015). <https://doi.org/10.1016/j.celrep.2015.07.001>
- 1098 82 Gallego-Carracedo, C., Perich, M. G., Chowdhury, R. H., Miller, L. E. & Gallego, J. A. Local field potentials  
1099 reflect cortical population dynamics in a region-specific and frequency-dependent manner. *Elife* **11**  
1100 (2022). <https://doi.org/10.7554/eLife.73155>
- 1101 83 Herreras, O. Local Field Potentials: Myths and Misunderstandings. *Front Neural Circuits* **10**, 101 (2016).  
1102 <https://doi.org/10.3389/fncir.2016.00101>
- 1103 84 Liu, Y. *et al.* Frequency Dependent Electrical Stimulation of PFC and ACC for Acute Pain Treatment in  
1104 Rats. *Front Pain Res (Lausanne)* **2**, 728045 (2021). <https://doi.org/10.3389/fpain.2021.728045>
- 1105 85 Dale, J. *et al.* Scaling Up Cortical Control Inhibits Pain. *Cell Rep* **23**, 1301-1313 (2018).  
1106 <https://doi.org/10.1016/j.celrep.2018.03.139>
- 1107 86 Baliki, M. N., Geha, P. Y., Fields, H. L. & Apkarian, A. V. Predicting value of pain and analgesia: nucleus  
1108 accumbens response to noxious stimuli changes in the presence of chronic pain. *Neuron* **66**, 149-160  
1109 (2010). <https://doi.org/10.1016/j.neuron.2010.03.002>
- 1110 87 Generaal, E. *et al.* Reduced hypothalamic-pituitary-adrenal axis activity in chronic multi-site  
1111 musculoskeletal pain: partly masked by depressive and anxiety disorders. *BMC Musculoskelet Disord* **15**,  
1112 227 (2014). <https://doi.org/10.1186/1471-2474-15-227>
- 1113 88 Wolock, S. L., Lopez, R. & Klein, A. M. Scrublet: Computational Identification of Cell Doublets in Single-  
1114 Cell Transcriptomic Data. *Cell Syst* **8**, 281-291 e289 (2019). <https://doi.org/10.1016/j.cels.2018.11.005>
- 1115 89 Hao, Y. *et al.* Integrated analysis of multimodal single-cell data. *Cell* **184**, 3573-3587 e3529 (2021).  
1116 <https://doi.org/10.1016/j.cell.2021.04.048>
- 1117 90 Korsunsky, I. *et al.* Fast, sensitive and accurate integration of single-cell data with Harmony. *Nat*  
1118 *Methods* **16**, 1289-1296 (2019). <https://doi.org/10.1038/s41592-019-0619-0>
- 1119 91 Traag, V. A., Waltman, L. & van Eck, N. J. From Louvain to Leiden: guaranteeing well-connected  
1120 communities. *Sci Rep* **9**, 5233 (2019). <https://doi.org/10.1038/s41598-019-41695-z>
- 1121 92 Furth, D. *et al.* An interactive framework for whole-brain maps at cellular resolution. *Nat Neurosci* **21**,  
1122 139-149 (2018). <https://doi.org/10.1038/s41593-017-0027-7>
- 1123
- 1124
- 1125

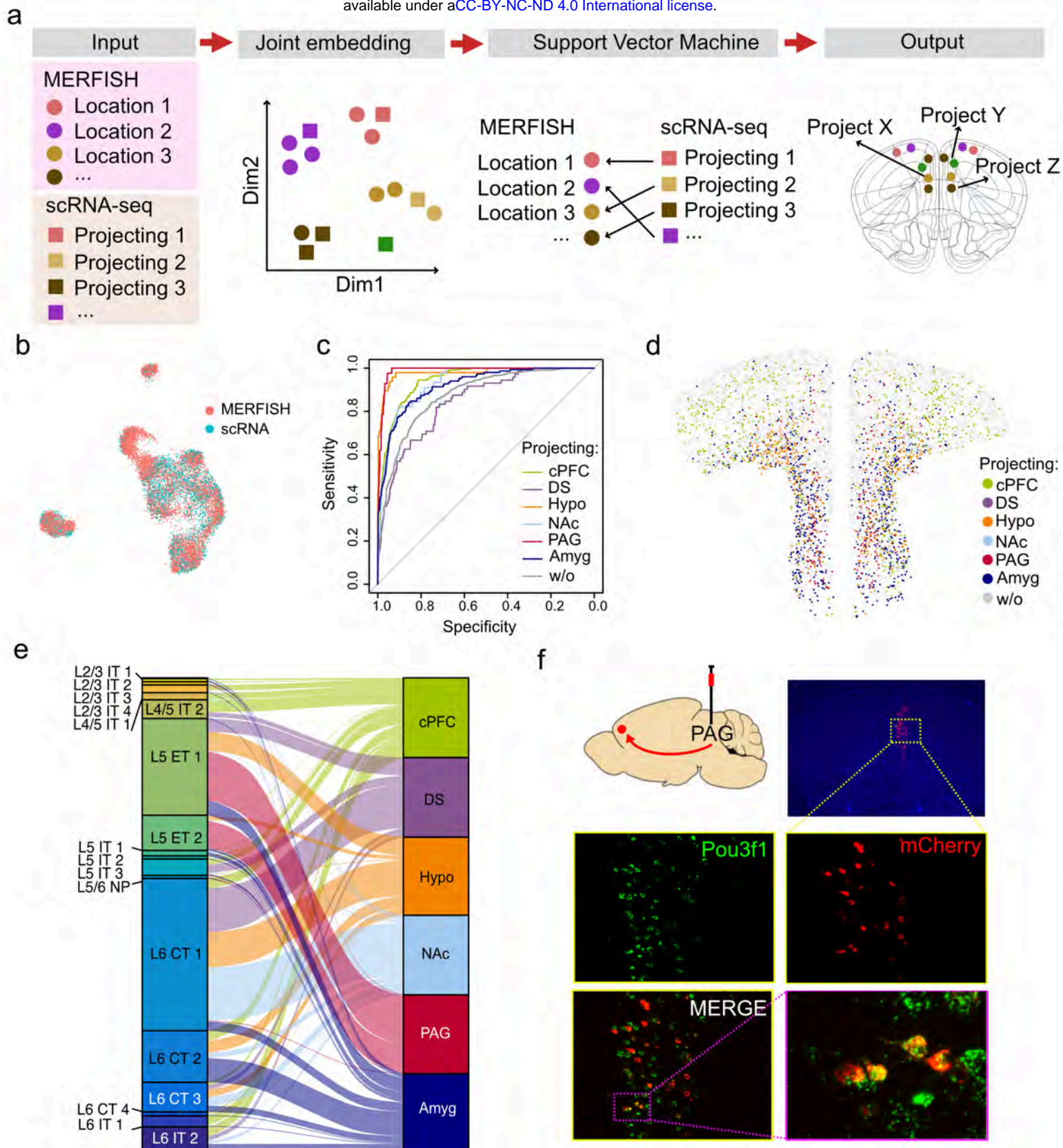


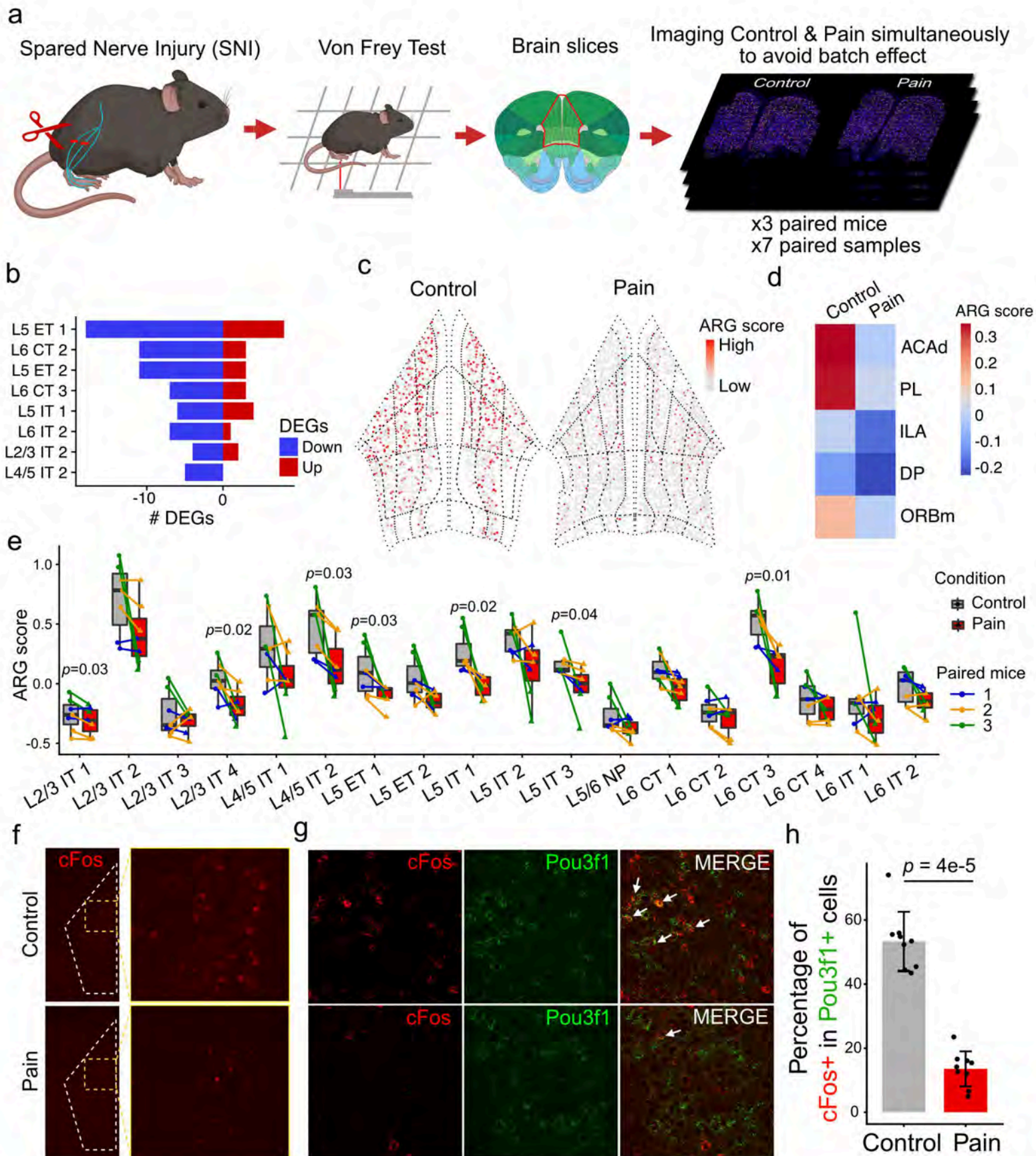


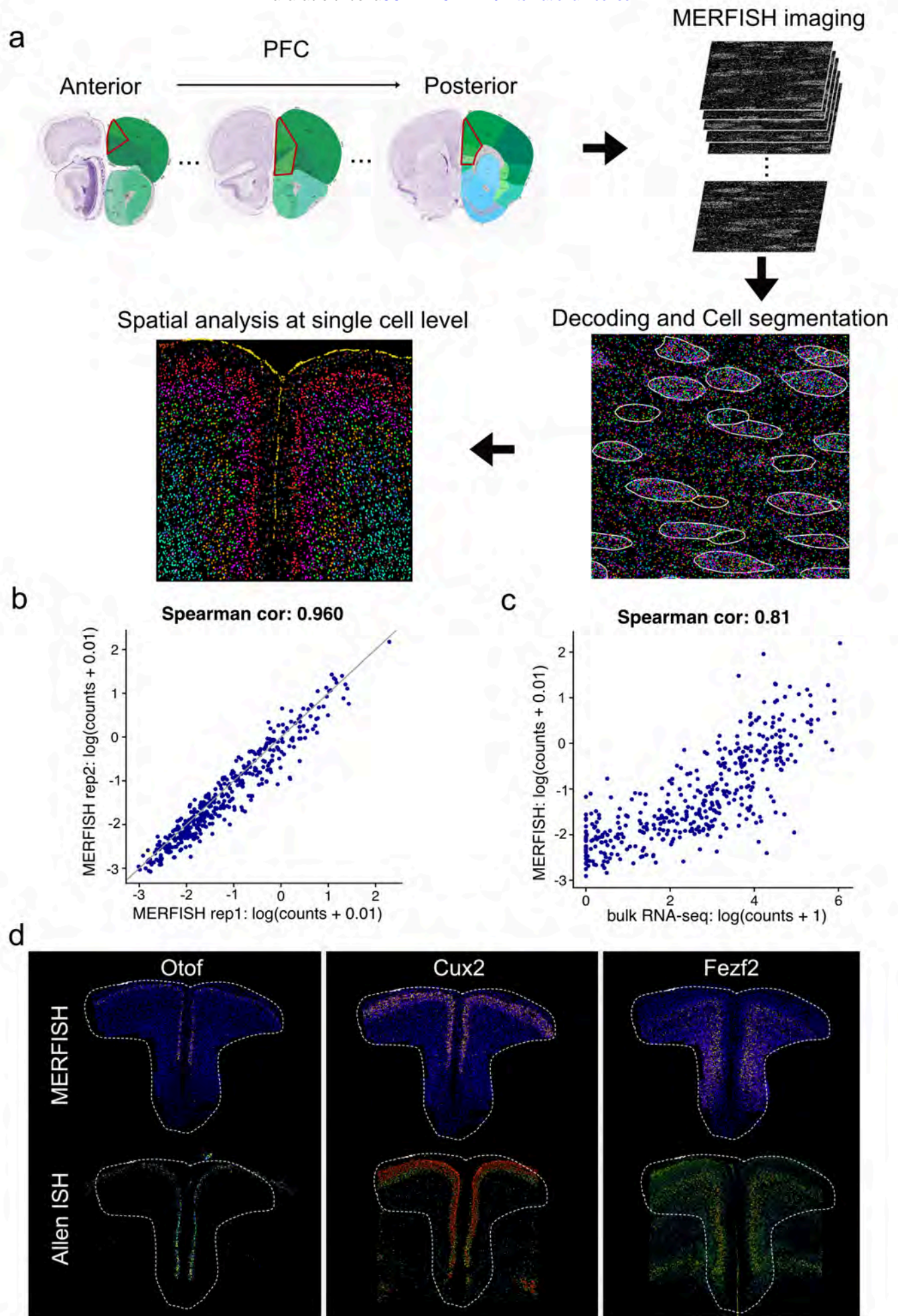


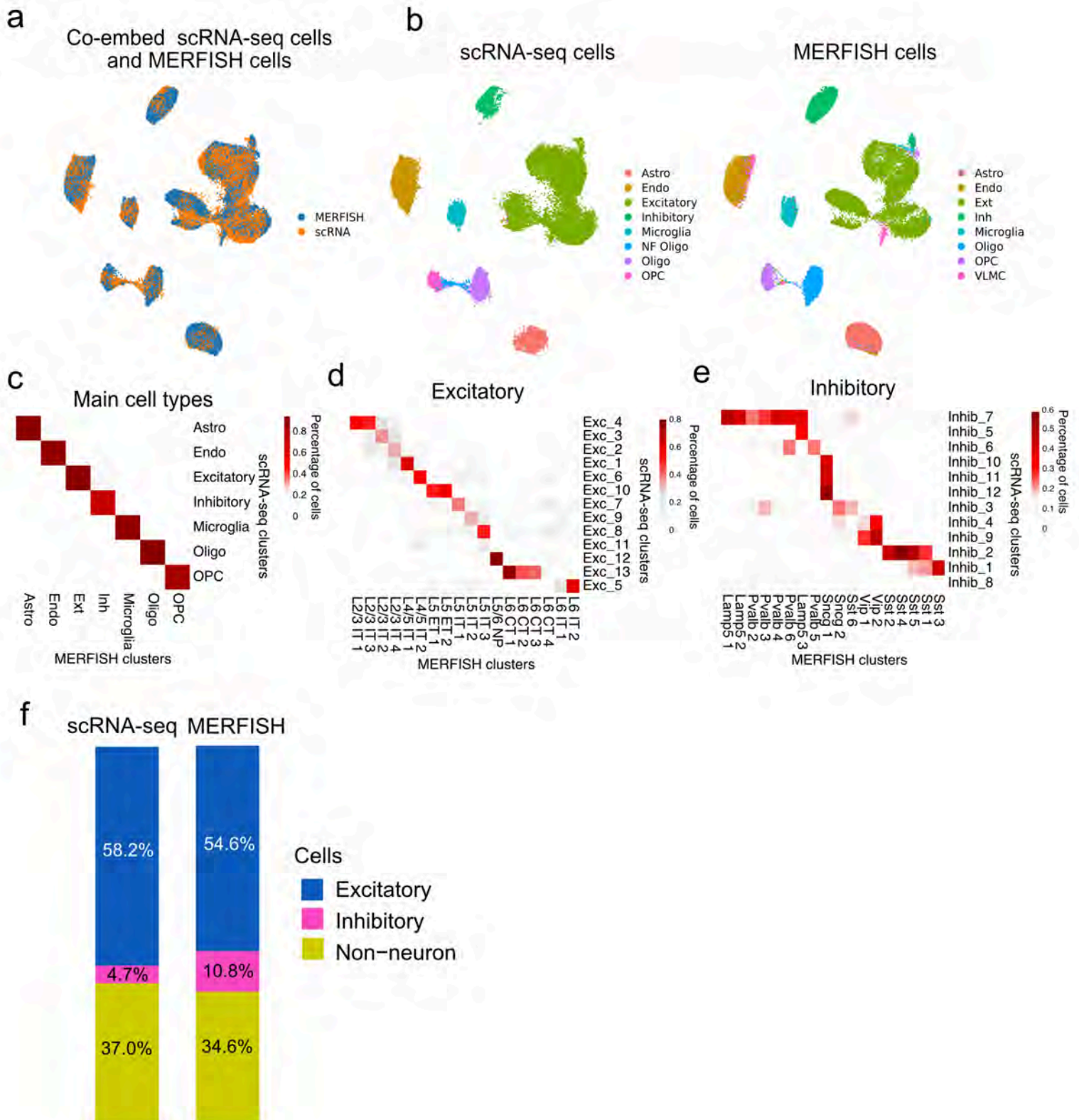




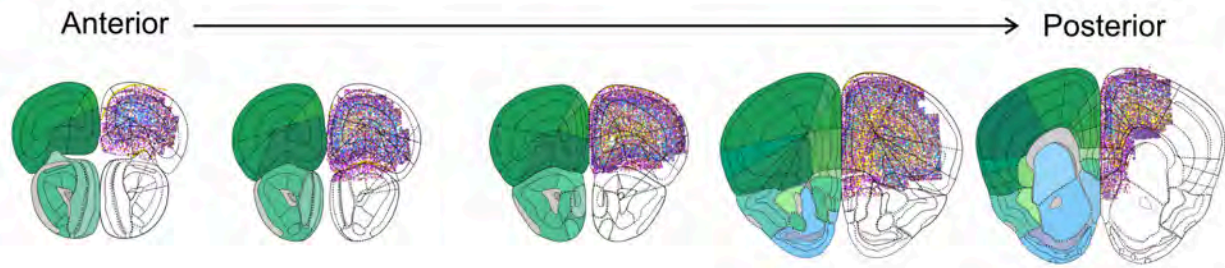




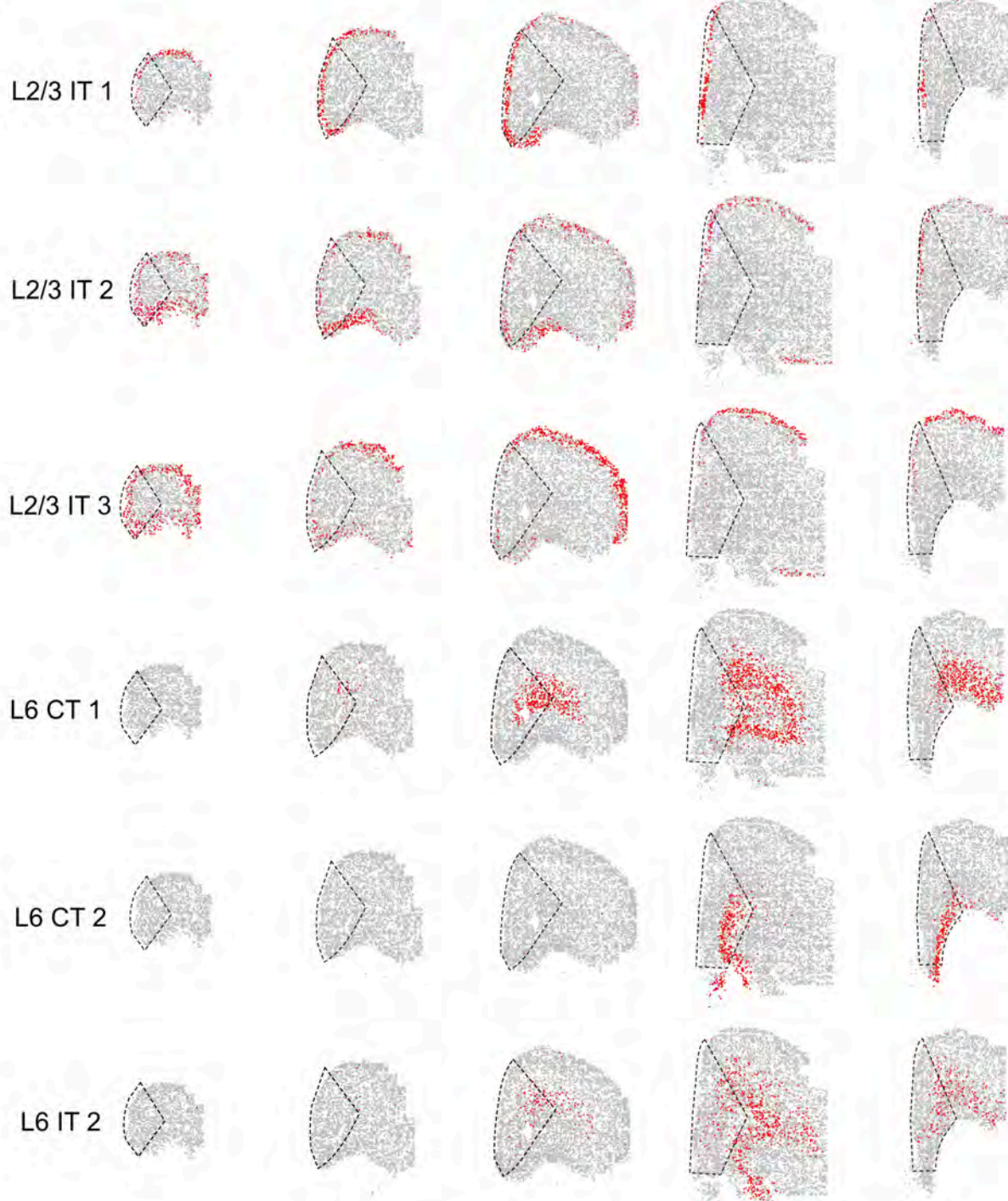


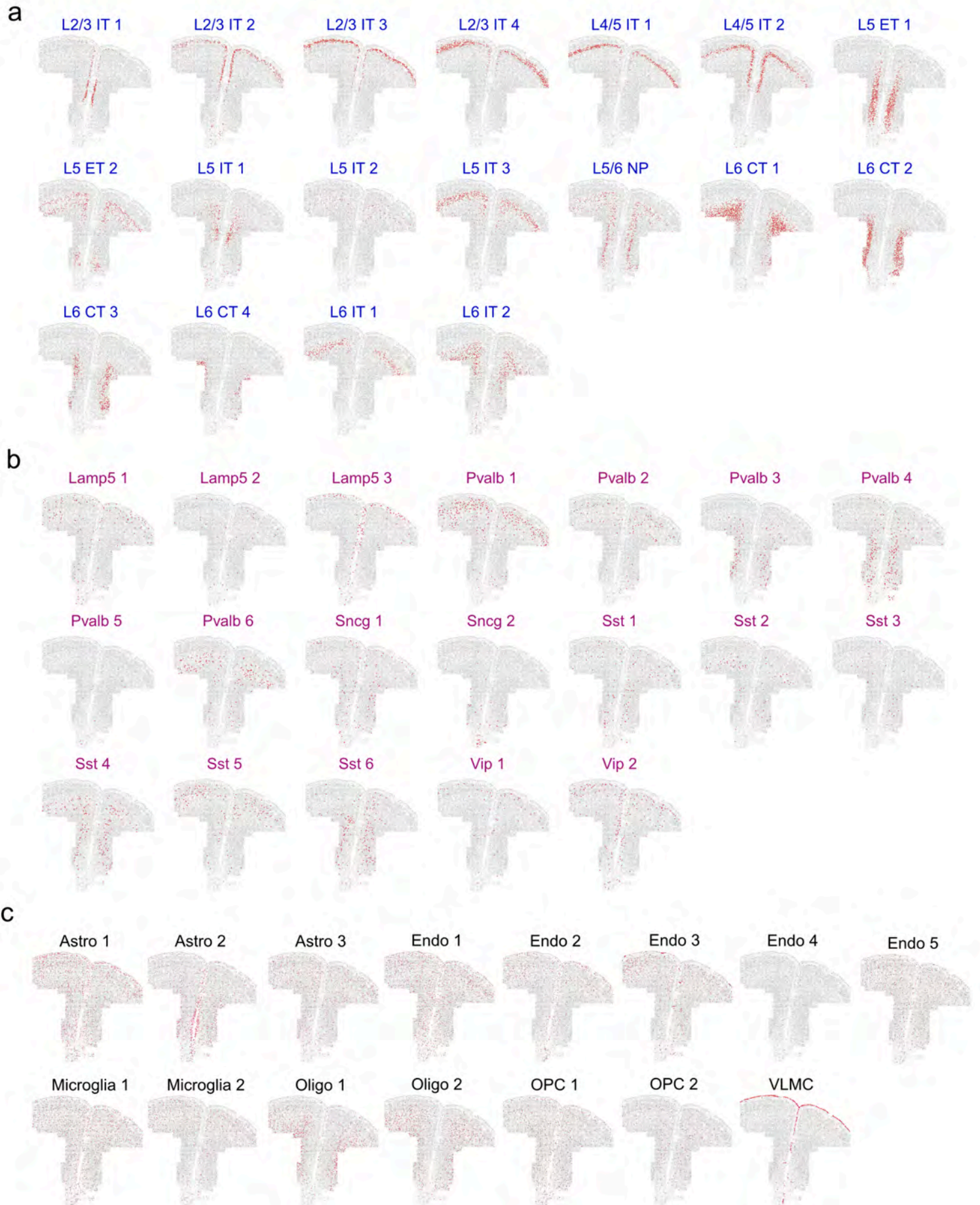


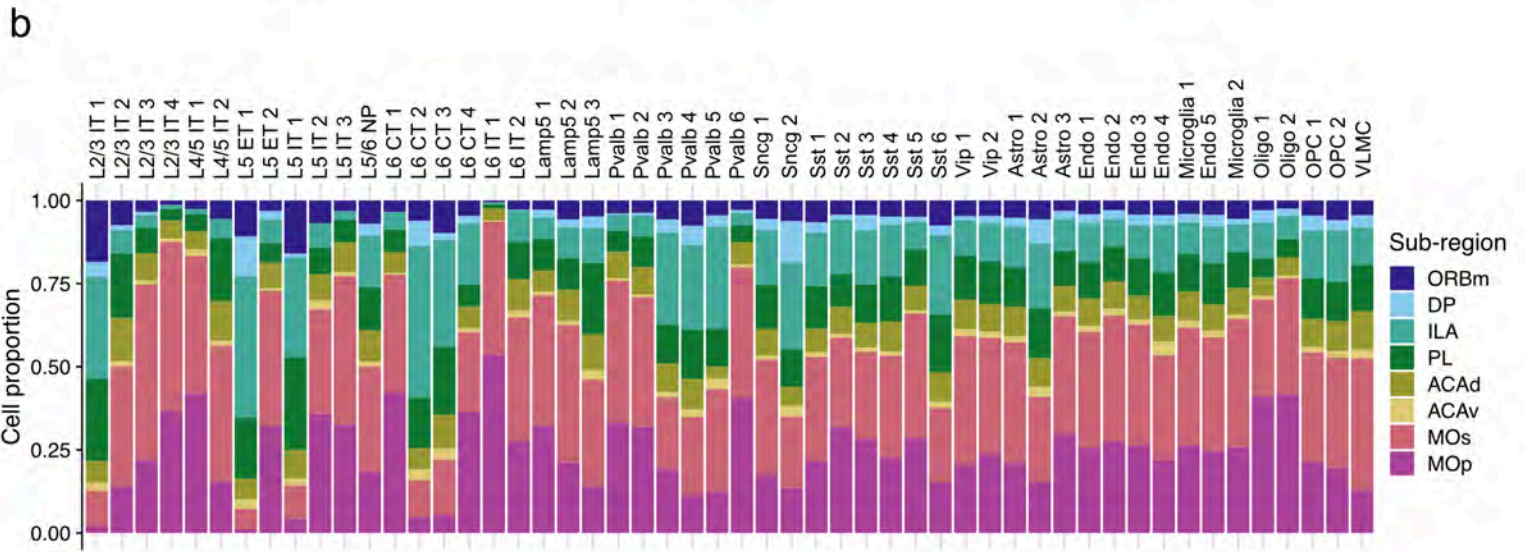
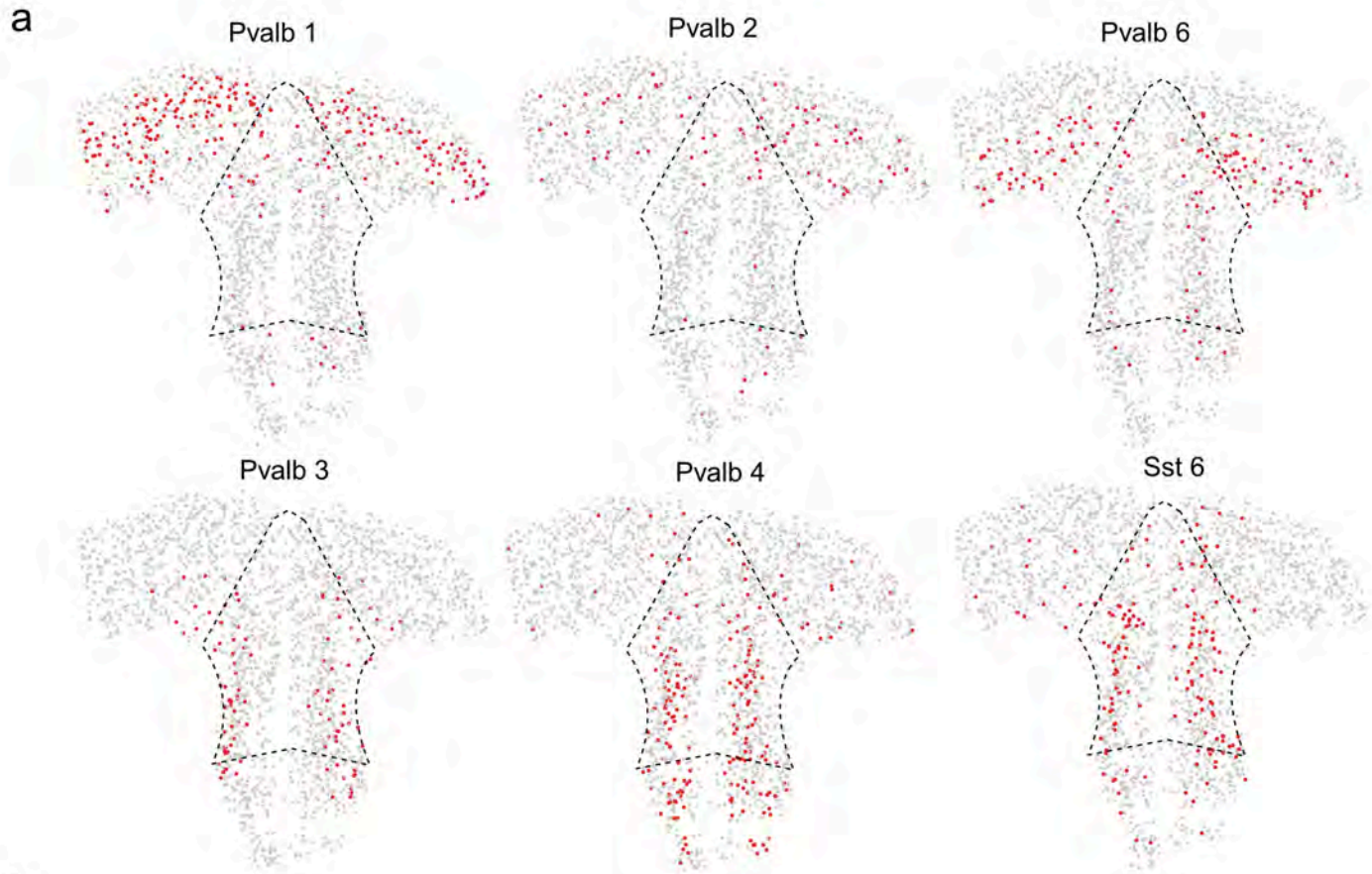
a

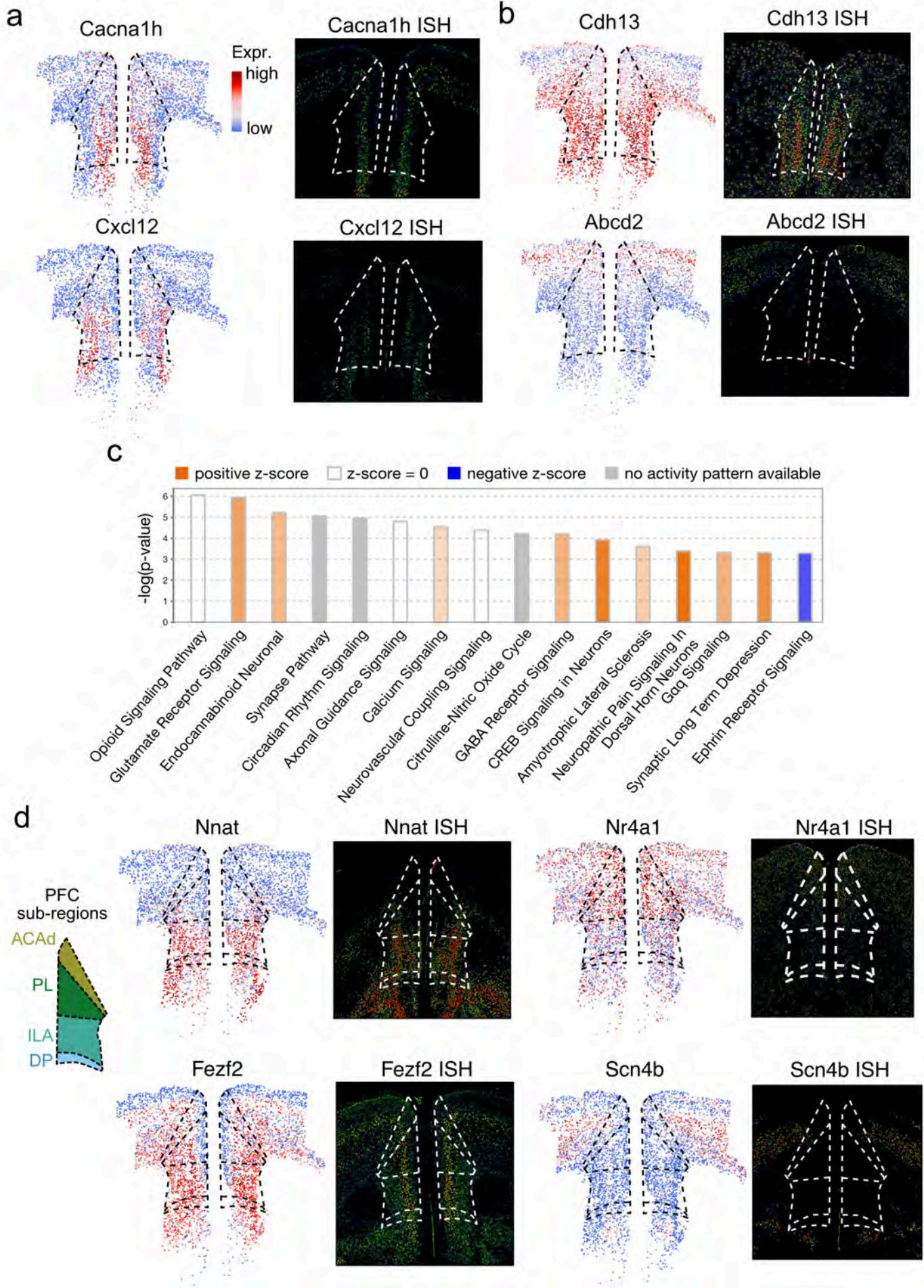


b



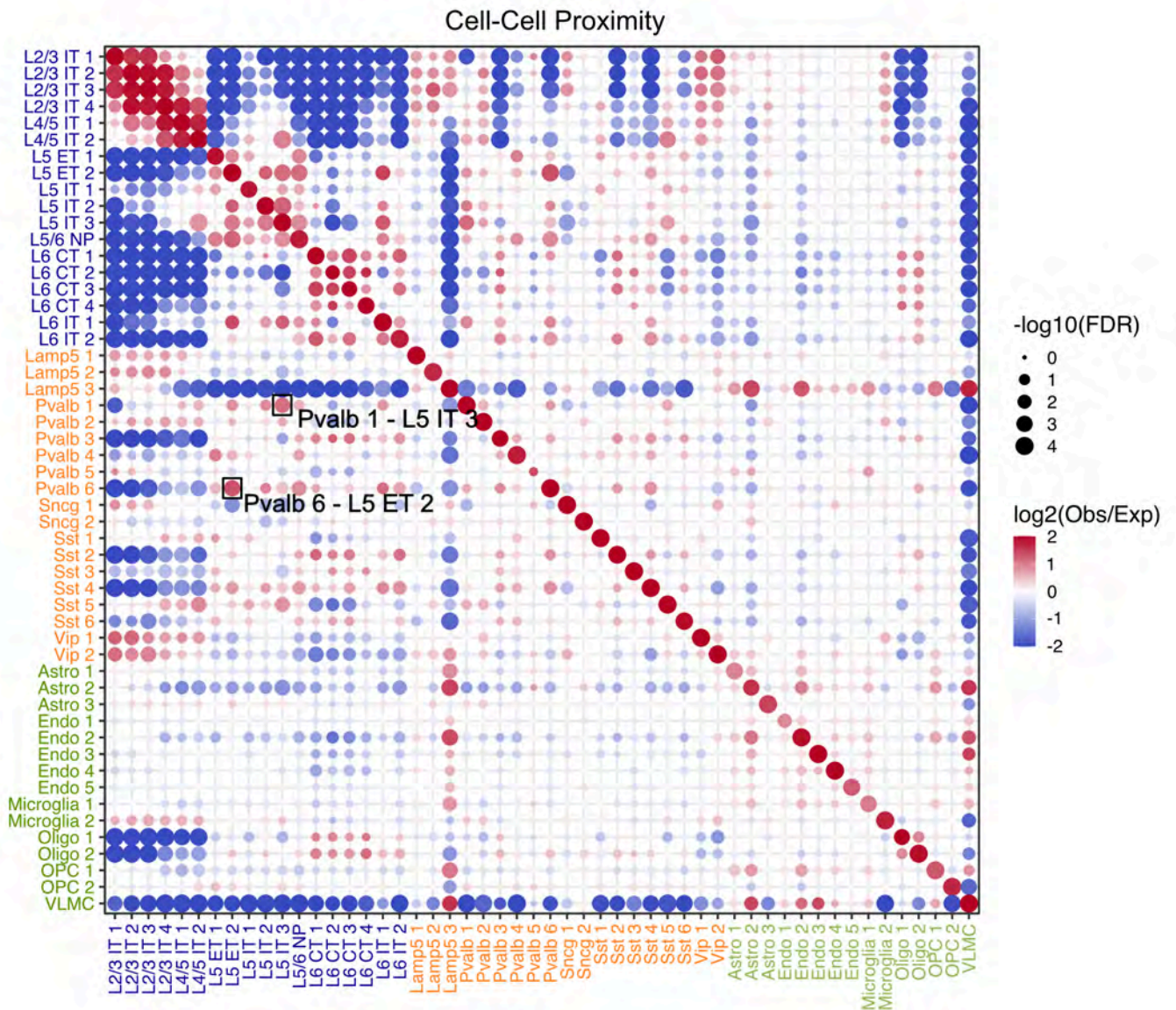








a



b

